The histone lysine demethylase KDM5C fine-tunes gene expression to regulate dendritic cell heterogeneity and function.

Hannah Guak[1,2*], Matthew Weiland[1*], Alexandra Vander Ark[1], Lukai Zhai[1], Kin Lau[3], Batsirai Mabvakure[1], Mario Corrado[1], Paula Davidson[1], Shelby Compton[1], Lisa DeCamp[1], Russell G. Jones[1], Sara M. Nowinski[1], Connie M. Krawczyk[1]

*authors contributed equally

[1]Department of Metabolism and Nutritional Programming, Van Andel Institute, Grand Rapids, MI 49503

[2] Department of Pediatrics, University of Michigan, Ann Arbor, MI 48109

[3]Bioinformatics and Biostatistics Core, Van Andel Institute, Grand Rapids, MI 49503

The functional and phenotypic heterogeneity of dendritic cells (DCs) plays a crucial role in facilitating the development of diverse immune responses that are essential for providing host protection. We found that KDM5C, a histone lysine demethylase of the KDM5 family regulates several aspects of conventional DC (cDC) and plasmacytoid DC (pDC) population heterogeneity and function. Using mice conditionally deficient in KDM5C in DCs, we found that loss of KDM5C results in an increase in Ly6C$^-$ pDCs compared to Ly6C$^+$ pDCs. We found that Ly6C$^-$ pDCs, compared to Ly6C$^+$ pDCs, have increased expression of cell cycle genes, decreased expression of activation markers and limited ability to produce type I interferon (IFN). Both KDM5C-deficient Ly6C$^-$ and Ly6C$^+$ pDCs have increased expression of activation markers, however are dysfunctional and have limited ability to produce type I IFN. For conventional cDCs, KDM5C deficiency resulted in increased proportions of cDC2Bs (CLEC12A$^+$, ESAM$^-$) and cDC1s, which was partly dependent on type I IFN and pDCs. Using ATAC-seq, RNA-seq, and CUT&RUN for histone marks, we found that KDM5C regulates epigenetic programming of cDC1. In the absence of KDM5C, we found an increased expression of inflammatory markers, consistent with our previous results in bone marrow-derived DCs. However, we also found a decrease in mitochondrial metabolism genes and altered expression of cDC lineage-specific genes. In response to *Listeria* infection, KDM5C-conditionally deficient mice mounted reduced CD8$^+$ T cell responses, indicating that KDM5C expression in DCs is necessary for their function. Thus, KDM5C is a key regulator of DC heterogeneity by modulating the balance of DC subsets and serves as a critical driver of the epigenetic programming and functional properties of DCs.

Introduction

Dendritic cells (DCs) are innate immune cells that play key roles in shaping innate and adaptive immunity. Like many immune cell types, DCs are a heterogeneous population comprising subsets that are classified based on ontogeny, transcriptional signatures, and functional properties. Their functional and phenotypic heterogeneity enables them to orchestrate customized immune responses that afford host protection against a diverse range of threats. Conventional or classical DCs (cDCs) are myeloid-derived and are functionally divided into two major subsets: cDC1 ($CD8^+XCR1^+$) and cDC2 ($CD4^+CD172a^+CD11b^+$). cDC2 can be further divided into cDC2A ($ESAM^+CLEC12A^-$) and cDC2B ($ESAM^-CLEC12A^+$), which are defined by the expression of the transcription factors T-BET and RORγt, respectively (1). cDC subsets are generally thought to arise from a common pool of pre-DCs that are committed to preferentially differentiate into cDC1 or cDC2 (2,3). cDCs are exceptionally efficient at presenting antigen to T cells, with cDC1s being specialized to cross-present antigens and stimulate $CD8^+$ T cell responses, whereas cDC2s promote $CD4^+$ T cell responses.

Another class of DC known as plasmacytoid dendritic cells (pDCs) can participate in T cell priming in some contexts, but they are primarily known for their capacity to produce large amounts of type I interferons (IFNs). Although less phenotypic heterogeneity has been described for pDCs, there is increased evidence of heterogeneity in the pDC population (4–6). In addition, pDC-like cells that possess characteristics of both pDCs and cDCs have been described in mice and humans (7–9). These cells have a transcriptional profile associated with pDCs but are poor producers of type I IFN and have an increased capacity for antigen presentation. Recent studies have used single-cell RNA-seq to better delineate DC ontogeny and have shown that pDCs are predominantly lymphoid in origin, although the precise contribution from the myeloid lineage is still debated (4,10,11). In fact, one recent study suggests that pDCs and cDC1s have a common precursor that is distinct from cDC2 precursors (11), and another identifies a pDC-like population that can give rise to cDC2Bs (12). Thus, the origins and differentiation trajectory of pDCs are still actively being defined, along with the mechanisms that guide DC fate.

Transcription factors such as Interferon Regulatory Factor (IRF) 8 and IRF4 are transcription factors that promote lineage specificity and function of pDCs and cDCs. IRF8 is required for the development of cDC1s as well as for the maintenance of cDC1 identity once differentiated (13). Although IRF8 is not required for pDC differentiation, it is essential for pDC function, including for type I IFN production (13). In contrast, IRF4 is not required for cDC1 or pDC differentiation and function but supports those of a subset of cDC2s (14,15). The amount of IRF8 or IRF4 is key for cDC identity, as high amounts of IRF8 is required for cDC1 identity, and high abundance of IRF4 can induce a similar transcriptional program including the majority of cDC1-specific genes (16).

Several transcriptional regulators in addition to IRF8 and IRF4 support epigenetic and transcriptional programming controlling DC specification (1,17–19). Deletion of these factors leads to either reduced production of a specific DC subset and/or a DC subset with abnormal identity (15,20–22). For example, deletion of the cDC1-specific factor BATF3 leads to the development of a cDC1-like subset that also displays cDC2-like properties (20). BATF3 maintains IRF8 autoactivation in cDC1-committed progenitors to support optimal cDC1 development (21). As well, production of cDC2B from pDC-like cells is dependent on KLF4 (12). Together these studies demonstrate the key role that transcription factors have in DC specification and function, but the role of chromatin modifiers such as KDM5C in these processes is poorly understood.

We previously found that the histone lysine demethylase KDM5C (SMCX, JARID1C) restrains bone marrow-derived DC (BMDC) activation *in vitro*, which was the first evidence that KDM5C is an important regulator of immune cell function (23). KDM5C removes permissive methyl groups from H3K4, thereby acting as a transcriptional repressor (24). In some instances, however, KDM5C has been associated with transcriptional activation (25,26). *Kdm5c* is an X-linked gene that escapes X-inactivation, so females express more KDM5C than do males(27). While a function for KDM5C in immune cells has not been described, KDM5C has been shown to regulate immune genes in non-immune cell types (28–31).

To better understand the function of KDM5C in DCs *in vivo,* we generated mice deficient in KDM5C in DCs (*Kdm5c*$^{\Delta Itgax}$ and *Kdm5c*$^{\Delta Zbtb46}$). We found that in the absence of KDM5C, pDC and cDC heterogeneity is altered. *Kdm5c*$^{\Delta Itgax}$ mice have an increase in Ly6C^{-} pDCs, which are poor producers of type I IFN. Both KDM5C-deficient Ly6C^{-} and Ly6C^{+} pDCs are also impaired in producing type I IFN. Additionally, *Kdm5c*$^{\Delta Itgax}$ mice display a specific increased proportion of cDC1 compared to cDC2, accompanied by an imbalance in cDC2 subsets, with a marked increase in cDC2Bs and decrease in cDC2A. Mechanistically, we found that KDM5C regulates epigenetic and transcriptional programming, leading to enhanced expression of inflammatory genes despite reduced DC function. Mitochondrial metabolism was altered in cDC1, and the expression of cDC1 lineage-specific genes including *Irf8* was reduced in KDM5C-deficient cDC1. *Kdm5c*$^{\Delta Itgax}$ mice had reduced CD8^{+} T cell responses to *Listeria* infection, demonstrating the requirement of KDM5C for cDC1 function. Together, our data show that the histone lysine demethylase KDM5C uniquely functions in DCs to regulate DC specificity and function.

Results

KDM5C regulates pDC heterogeneity.

Previously, we have shown that KDM5C cooperates with PCGF6 to restrain BMDC steady-state activation (23). To investigate the function of KDM5C in DCs *in vivo*, we generated mice with KDM5C deleted in pDC and cDCs (*Itgax-Cre-Kdm5c*$^{fl/fl}$*; Kdm5c*$^{\Delta Itgax}$), and examined the abundance and proportions of DC populations in the spleen (**Figs. 1, S1**). Within the pDC population (Lineage(B220$^+$CD3$^+$Ly6C$^+$CD19$^+$NK1.1$^+$) SiglecH$^+$CD11c^{int}CD11b$^-$PDCA1$^+$), we discovered that a significant proportion of splenic pDCs in the *Kdm5c*$^{\Delta Itgax}$ mice did not express Ly6C. This Ly6C$^-$ population was increased > 4-fold compared to the controls (**Fig 1A**). The proportion of splenic Ly6C$^+$ pDCs was lower in *Kdm5c*$^{\Delta Itgax}$ due to the increase in Ly6C$^-$ pDCs, although the cell count was unchanged (**Fig 1A**).

To further describe Ly6C$^-$ pDCs, we examined activation marker expression and found that Ly6C$^-$ pDCs have significantly lower expression of the surface markers typically associated with DC activation, including CD86, CD80, MHCII, PD-L1, and CD40, compared to Ly6C$^+$ pDCs (**Fig 1B**). We examined transcriptional differences between Ly6C$^+$ and Ly6C$^-$ pDCs using RNA-seq and found that Ly6C$^-$ pDCs have increased enrichment of genes associated with the cell cycle, whereas Ly6C$^+$ pDCs have increased enrichment of C-type lectins and IL-4 and IL-13 signaling (**Fig 1C**). While pDCs are terminally differentiated and are known to have low proliferation potential (32), these data suggest that the Ly6C$^-$ pDCs still have proliferative capacity and are less mature. CD4$^-$ pDCs have been shown to be a less mature subset of pDC (32); we therefore examined whether Ly6C expression correlates with CD4 expression on pDCs. Ly6C$^-$ and CD4-expressing cells do not co-segregate; however, Ly6C$^+$ pDCs have a greater proportion of CD4$^+$ cells compared to Ly6C$^-$ pDCs (**Fig 1D, left**). Further, bone marrow, where pDC development takes place, contains a larger frequency of Ly6C$^-$ pDCs compared to those found in the spleen (**Fig 1D, right**). These data suggest Ly6C$^-$ pDCs are less mature than Ly6C$^+$ pDCs.

To determine if pDC populations change following immune activation, we examined pDC populations in uninfected controls and mice infected with lymphocytic choriomeningitis virus (LCMV) for 20 hours. We found that very few Ly6C$^-$ pDCs were present in the spleen. (**Fig 1E**). Because type I IFN feedback is known to be important for pDC function (33), we tested whether type I IFN is required for the steady state populations of Ly6C$^-$ and Ly6C$^+$ pDC by examining mice deficient for IFNAR1 (*Ifnar1*$^{-/-}$), the receptor for IFN-α and IFN-β. *Ifnar1*$^{-/-}$ mice had less splenic Ly6C$^+$ pDCs and more Ly6C$^-$ pDCs compared to the wild-type (WT) controls (**Fig 1F**). In line with these results, the generation of Ly6C$^+$ pDCs was enhanced by the addition of IFN-β during *in vitro* differentiation of bone marrow precursors to DCs with FLT3L (**Fig 1G**). To test the functionality of Ly6C$^-$ pDC, we measured their

ability to produce type I IFN following TLR9 stimulation. We found that Ly6C$^-$ pDC produced less IFN-α compared to Ly6C$^+$ pDCs (**Fig 1H**). As well, about half of the Ly6C$^-$ pDC became Ly6C$^+$ following TLR9 stimulation (**Fig 1I**). Together, these findings suggest that type I IFN affects the balance of Ly6C$^{-/+}$ pDCs and that Ly6C$^-$ pDCs may be a less mature subpopulation of pDCs.

To determine how KDM5C deficiency impacts pDC phenotype, we examined activation markers by flow cytometry. KDM5C-deficient animals had increased expression of the activation markers CD80, MHC-II, and CD40 in both Ly6C$^+$ and Ly6C$^-$ pDCs, and increased PD-L1 expression by Ly6C$^+$ pDCs, compared to controls (**Fig 2A**). We generated bone marrow chimeras to test whether the proportions of Ly6C$^-$ and Ly6C$^+$ pDC are due to intrinsic factors or can be rescued by a WT environment and/or WT pDCs. We reconstituted the bone marrow of CD45.1 mice (WT) with either an equal mix of CD45.1$^+$ control bone marrow cells and CD45.2$^+$ *Kdm5c$^{\Delta Itgax}$* cells (KO), or of CD45.2$^+$ *Kdm5c$^{\Delta Itgax}$* cells alone. In a WT environment with and without WT pDC, *Kdm5c$^{\Delta Itgax}$* bone marrow produced similar proportions of Ly6C$^-$ and Ly6C$^+$ pDCs compared to *Kdm5c$^{\Delta Itgax}$* mice (**Fig 2B**). Similarly, activation markers expressed on KO Ly6C$^{+/-}$ pDCs that developed in a WT environment remained at levels of *Kdm5c$^{\Delta Itgax}$* alone (**Fig 2B**). Therefore, we conclude that Ly6C$^-$ pDC population size is intrinsically regulated by KDM5C.

We examined how KDM5C deficiency affects transcriptional programming in pDCs by comparing the transcriptomes of control and KDM5C-deficient Ly6C$^-$ and Ly6C$^+$ pDCs from mice injected with PBS or LCMV (**Fig 2C**). In response to LCMV (20 hours), KDM5C-deficient pDCs had increased expression of genes involved in antigen presentation, interferon signaling (IFI genes), and cytokine signaling, suggesting increased immune activation (**Fig 2D, E and S2**). We also found enrichment of genes involved in negative regulation of the immune system (**Fig 2E**). Because we found increased gene expression of genes that both positively and negatively regulate immune responses, we tested the function of KDM5C-deficient pDCs. In response to TLR9 stimulation, KDM5C-deficient Ly6C$^+$ pDCs produced significantly less IFN-α compared to controls (**Fig 2F**). Thus, in the absence of KDM5C, pDCs have an activated transcriptional profile and cell surface phenotype but fail to produce type I IFN upon stimulation.

KDM5C regulates cDC heterogeneity.

Our initial DC population profiling experiments included cDCs (Lineage$^-$CD64$^-$MHCII$^+$CD11c$^+$ CD26$^+$) at homeostasis and we discovered that loss of KDM5C also impacts cDC heterogeneity. The proportion and number of cDC1s (XCR1$^+$) and cDC2Bs (CD172a$^+$ESAM$^-$CLEC12A$^+$) and merocytic DCs (XCR1$^-$CD172a$^-$) were higher in *Kdm5c$^{\Delta Itgax}$* mice compared to control mice (**Fig 3A**), whereas cDC2As (ESAM$^+$CLEC12A$^-$) were lower (1,5,34,35). The proportional changes were largely due to a decrease in cDC2A numbers **(Supplementary Fig 3A**).

Cre expression under the control of the CD11c promoter is not exclusive to cDCs, and also includes expression in pDCs, as detailed above, along with some macrophages (36); therefore, to examine the effects of KDM5C deletion specifically in cDCs, we generated mice with KDM5C deleted in ZBTB46-expressing cells (*Kdm5c*$^{\Delta Zbtb46}$). Comparison of cDC1 versus cDC2 populations in *Kdm5c*$^{\Delta Zbtb46}$ mice showed similar trends as *Kdm5c*$^{\Delta Itgax}$ mice (**Fig 3B**); however, the magnitude was less than that observed in the *Kdm5c*$^{\Delta Itgax}$ mice. Further, cDC2A and cDC2B proportions were not affected by *Kdm5c* deletion in *Kdm5c*$^{\Delta Zbtb46}$ mice (**Fig 3B**). We examined KDM5C deletion by western blot and found that KDM5C deletion was more efficient in *Kdm5c*$^{\Delta Itgax}$ DCs compared to *Kdm5c*$^{\Delta Zbtb46}$ DCs (**Supplementary Fig 3B**). There are several possibilities as to why these two models differ. *Cd11c-Cre* and *Zbtb46-Cre* are both expressed in the pre-cDC stage(36); however, the relative timing of their expression has not been accurately determined. In addition to differences in timing of Cre transgene expression and deletion efficiency, the difference in the cDC2 populations in the *Kdm5c*$^{\Delta Zbtb46}$ and *Kdm5c*$^{\Delta Itgax}$ mice could be a result of environmental differences due to KDM5C deletion in other cell types, since *Cd11c-Cre* expression is less restricted than *Zbtb46*-Cre.

Because KDM5C deficiency in *Cd11c*-expressing cells results in altered pDCs, we examined whether the altered pDCs contributed to the differences in cDC heterogeneity. We first depleted pDCs in wild type mice by administering 250 µg of anti-PDCA-1 antibody intraperitoneally every other day for one week *in vivo* (**Supplementary Fig 3C,D**). Depletion of pDCs resulted in a small but significant increase in the proportion of cDC2B relative to cDC2A (**Fig 3C**), but without the changes in cDC1 and cDC2A population sizes seen in the *Kdm5c*$^{\Delta Zbtb46}$ and *Kdm5c*$^{\Delta Itgax}$ mice (**Fig 3C; Supplementary Fig 3F)**. These results were reproduced in *Ifnar*-deficient mice, indicating that pDCs and type I IFN contribute moderately to changes in proportions of cDC2 subsets, but not cDC1s (**Fig 3D; Supplementary Fig 3G**). To further examine the effects of the environment on cDC heterogeneity, we generated bone marrow chimeric mice as in Fig 1B and 2B. We found that, similar to our findings for pDCs, the population dynamics of KDM5C-deficient cDCs were retained in the presence of WT hematopoietic cells (mixed chimera) and in the WT environment (**Fig 3E**), demonstrating that KDM5C deletion has both intrinsic and extrinsic effects on cDC population heterogeneity.

KDM5C controls gene expression in cDC at homeostasis

We performed RNA-seq on control and KDM5C-deficient cDC1, cDC2A and cDC2B. KDM5C deletion resulted in the greatest effects on cDC1 (~2000 differentially expressed genes) compared to ~600 and ~800 DE genes in cDC2A and cDC2B, respectively. KDM5C-deficient cDC1s displayed enrichment of transcripts encoding proteins in inflammatory pathways, cytokine pathways, defense to viral infection, immune cell activation and IRF regulated pathways (**Fig 4A,B, S4A, B, C**). These data are consistent

with our previous work in BMDCs showing that KDM5C restrains DC activation (23). We performed transcription factor binding site analysis using Hypergeometric Optimization of Motif EnRichment (HOMER) on genes with significantly increased expression levels in KDM5C-deficient cDC1s compared to control, and found predominant enrichment of IRF family TF motifs (**Fig 4C**). This agreed well with our RNA-seq data which indicated the dysregulation of several *Irf* genes in the absence of KDM5C (**Fig 4D Heatmap**). Specifically, *Irf7*, *Irf1, Irf4* and *Irf2bpl* were significantly upregulated in KDM5C-deficient cDC1 compared to controls. IRF proteins are well known to participate in DC activation and activate inflammatory pathways, and therefore are likely key mediators of the increased gene expression observed in KDM5C-deficient cDC1.

KDM5C modifies chromatin structure by regulating the levels of H3K4me3, a histone PTM associated with active chromatin state and gene transcription. We examined H3K4me3 levels by Cleavage Under Targets and Release Using Nuclease (CUT&RUN)[19,26] on ~20K sorted cells of each subset. We found that global H3K4me3 levels increased in KDM5C-deficient cDC1s consistent with KDM5C being an H3K4 demethylase. The majority of the differentially methylated regions were found in intergenic regions (**Fig S4D**). To understand how changes in H3K4 trimethylation correspond to changes in gene expression in KDM5C-deficient DCs, we analyzed H3K4me3 levels in genes that were up or down regulated in our RNA-seq analysis (**Fig 4E).** As expected, we found increased H3K4me3 in genes that were upregulated in KDM5C-deficient cDC1s (**Fig 4E**). Surprisingly, we also found increased H3K4me3 associated with genes that showed decreased expression (**Fig 4E**). Regions with increased H3K4me3 were found in genes associated with immune cell migration, and proliferation (**Fig 4F**). Genes that were upregulated, such as *Ifi27* and *Il10*, were commonly associated with increased H3K4me3, chromatin accessibility (ATAC-seq) and H3K27ac (a marker of active chromatin) (**Fig 4G**). Genes such as *Cd207* that were downregulated had decreased chromatin accessibility and H3K4me3, whereas decreased expression of other genes such as *Ccr9* did not show corresponding changes in H3K4me3, chromatin accessibility or H3K27ac (**Fig 4G**). Together, these data support our model in which KDM5C restricts DC activation through the specific demethylation and inactivation of promoters of pro-inflammatory genes, including many IRF genes.

KDM5C regulates OXPHOS gene expression and mitochondrial function in cDC1.

As shown in **Fig 4E**, pathway enrichment analysis of our RNA-seq data identified the decreased abundance of transcripts associated with mitochondrial metabolism, including oxidative phosphorylation, in KDM5C-deficient cDC1s. Since bioenergetic metabolism is important for the function of DCs (37–40), we next examined the expression of genes encoding factors involved in oxidative phosphorylation and found that many genes were significantly decreased in KDM5C-deficient cDC1s (**Fig 5A**). To determine

if altered expression of mitochondrial metabolism genes results in altered mitochondrial function, we first analyzed mitochondrial content and membrane potential using the mitochondrial dyes MitoSpy Green and TMRM, respectively. We found that with KDM5C deficiency, mitochondrial mass was lower, as was mitochondrial membrane potential (**Fig 5B)**. However, when graphed as a ratio, KDM5C-deficient cDC1 had increased membrane potential relative to mitochondrial mass. These differences were not due to changes in cell size (**Supplementary Fig 5A**).

To assess whether these changes in mitochondria resulted in differences in cellular bioenergetics, we used a Seahorse bioanalyzer to measure cellular respiration. Surprisingly, we found that KDM5C-deficient cDC1s had a comparable baseline oxygen consumption rate (OCR) compared to the control, despite reduced mitochondrial mass (**Fig 5C**). Seahorse analysis uses the addition of several mitochondrial inhibitors to test the contribution of various mitochondrial processes to cellular OCR and provide insights into the causes of mitochondrial dysfunction. Oligomycin addition blocks the F_1F_0-ATPase and thus leftover OCR is due to proton leak into the mitochondrial matrix and/or non-mitochondrial respiration. KDM5C-deficient cDC1s displayed similar OCR following oligomycin treatment, however had increased non-mitochondrial respiration, suggesting that KDM5C-deficient cells have lower levels of proton leak (**Fig 5C**). Reduced proton leak can cause an increase in proton build up in the intermembrane space, and likely explains the enhanced mitochondrial membrane potential per mass that we observed using TMRM and MitoSpy Green. Since proton leak occurs passively or actively through uncoupling proteins (UCPs), we examined gene expression of UCPs in cDC1, and found a decrease in the expression of UCP2 (p.adj. 1.08E-06), potentially explaining the reduced levels of proton leak.

Spare respiratory capacity (SRC) is commonly assessed by measuring OCR following the addition of the mitochondrial uncoupler FCCP, which allows the release of protons from the inter membrane space, and results in maximal oxygen consumption as the mitochondria attempt to replenish membrane potential. We found there was a significant increase in SRC in the *Kdm5c*$^{\Delta Itgax}$ vs control cDC1s, which is again consistent with the increased TMRM/Mitospy Green ratio that we observed (**Fig. 5B,C**). Together, these data support a model in which, in the absence of KDM5C, changes in gene expression of OXPHOS genes and UCP2 result in lower overall mitochondrial mass, but increased mitochondrial membrane potential per mitochondria, and elevated SRC. These data also suggest that mitochondrial oxygen consumption is tightly coupled to ATP production in KDM5C-deficient cDC1s.

We examined H3K4me3 levels of OXPHOS genes with reduced expression in KDM5C-deficient cDC1. Surprisingly, we found that decreased expression was not associated with decreased H3K4me3 or decreased H3K27ac, a marker of active gene expression **Figs 5D, E**. We performed HOMER analyses on

the same genes and found enrichment for YY1 motifs (**Fig S5B**). YY1 promotes the expression of mitochondrial respiration genes (41) through interaction with PGC-1α. All together, these data strongly support a model in which KDM5C is a key regulator of mitochondrial function in cDC1s.

KDM5C expression in DCs is required for T cell response to *Listeria* infection.

In **Fig 4G** we showed that KDM5C results in altered gene expression of several IRF family members, including *Irf4* and *Irf8,* which encode lineage specifying transcription factors required for the generation and function of cDC1 and cDC2, respectively. We examined the expression of several lineage markers in cDC1s and found decreased expression of several cDC1-specific genes including *Irf8*, *Xcr1*, *Batf3*, *Cadm1*, and an increase in cDC2-specific genes including *Ltb*, *Cd4*, *Irf4*, *Itgam*, and *Tbx21*. Further, expression of *Tbx21*, which encodes cDC2A-specific transcription factor T-BET, was reduced in cDC2As to levels found in cDC2B (**Fig 6A**). Like the mitochondrial genes, changes in gene expression were not strongly associated with changes H3K4me3 or H3K27ac (**Fig 6B**). We however confirmed decreased IRF8 expression by flow cytometry (**Fig. 6C**). Thus, lineage specifying transcriptional programs are altered in the absence of KDM5C. Lineage-specific transcriptional programs are important for DC identity, differentiation, and function. To test whether the function of DCs is altered in the absence of KDM5C, we used the *Listeria monocytogenes* infection model in which proper cDC1 abundance and function are crucial for activating $CD8^+$ T cells (42). Control and *Kdm5c*$^{\Delta Itgax}$ mice were infected with *Listeria monocytogenes* expressing ovalbumin (LM-OVA) for 7 days. Following infection with LM-OVA, the altered proportions of cDC and pDC subsets remained similar to those at homeostasis (**Fig 1A,B**), with *Kdm5c*$^{\Delta Itgax}$ mice exhibiting increased proportions of cDC1, cDC2B, and $Ly6C^-$ pDCs, and decreased proportions of cDC2A and $Ly6C^+$ pDCs in (**Supplementary Fig 6A,B**). Although there were no significant differences between control and *Kdm5c*$^{\Delta Itgax}$ mice in $CD11a^+CD49d^+$ antigen-experienced or $CD44^+$ effector $CD4^+$ T cells (**Fig 6F**), the proportion of *Listeria*-specific $CD8^+$ T cells (tetramer$^+$) was reduced in *Kdm5c*$^{\Delta Itgax}$ mice (**Fig 6D**). In addition, *Kdm5c*$^{\Delta Itgax}$ $CD8^+$ T cells were less functional, as measured by decreased IFN-γ^+ and IFN-γ^+ TNF-α^+ polyfunctional $CD8^+$ T cell populations (**Fig 6E**). Thus, KDM5C expression in DCs is necessary for CD8 T cell response to infection.

Discussion

Immune protection requires that immune responses be tailored to the infection or insult. DCs are among the first responders, and as a whole are specialized in antigen presentation and cytokine production. However, several subsets exist within the DC population whose functions are further specialized. Significant advances of the mechanisms that guide DC specification into these subsets are

continuously being made (4,5,11,12,18,43). While several transcription factors have been demonstrated to be important for DC specification (17,18,44,45), our results show that histone modifying enzymes also influence DC cell fate. Our work implicates KDM5C as a key regulator of the balance of both pDC and cDC subtypes. In the absence of KDM5C, pDC and cDC population heterogeneity is altered and functions of both cell populations is impaired. KDM5C is not, however, required to generate a specific subset. Rather, it alters the proportions of subsets through modifying the epigenome and gene expression. Our data show that KDM5C is also important for functional responses of pDC and cDC, and that mice without KDM5C in DCs mount impaired $CD8^+$ T cell response to *Listeria* infection.

Here, we identified a population of pDC that are $Ly6C^-$, and are more prevalent in *Kdm5c*$^{\Delta Itgax}$ mice. $Ly6C^-$ pDC are not well-studied, although one study also suggests that they produce less type I IFN than $Ly6C^+$ cells (46). Recent studies have begun to highlight the heterogeneity and diverse functions of pDCs. Murine pDC-like ($Lin^-BST2^+SiglecH^+ZBTB46^+$) cells and transitional DCs (tDCs) ($Lin^-CD11b^{low}CD11c^+SiglecH^+CX3CR1^-PDCA1^+$) resemble pDCs but share some characteristics and transcriptional similarities to cDCs(12,43). The pDC-like population has been described to serve as a progenitor pool for cDC2s(12). The specialized tDC exhibits an enhanced capacity for antigen presentation compared to pDCs and limited ability to produce type I IFNs, and can be further divided into $CD11c^{low}$ tDC ($Ly6C^+$), and CD11c high tDC ($Ly6C^-$)(43). Although the $Ly6C^-$ pDCs that were enriched in *Kdm5c*$^{\Delta Itgax}$ mice in our study had impaired type I IFN production, they were not exactly equivalent to the pDC-like or tDCs described in these other studies. Several lines of evidence from our work suggest that $Ly6C^-$ pDCs are an immature pDC population: they have increased expression of cell cycle genes; their abundance is greater in the bone marrow, where pDC maturation occurs; and infection, IFN-β, and TLR-9 agonists induce a significant proportion of $Ly6C^-$ pDC to become $Ly6C^+$. Previous studies showed that $CD4^+$ pDC are less migratory and produce lower levels of cytokines in response to stimulation compared to $CD4^-$ pDC (32). However, in our data, Ly6C and CD4 expression did not co-segregate, suggesting they are not the same populations. This raises the possibility that there may be subsets within the $Ly6C^-$ population. Further analyses at the single cell level are needed to understand the relationship between these subsets.

KDM5C-deficient $Ly6C^+$ pDCs have an activated phenotype but are dysfunctional, which is a phenotype similar to that of exhausted pDCs (47,48). Exhausted pDCs have been found in models of persistent viral infections, have an activated phenotype, and fail to produce type I IFN upon CpG stimulation (48). KDM5C-deficient pDCs have an increase in expression of immune genes associated with activation, including *Ifi27*, *Ifi30*, MHCI and MHCII, as well as increased expression of several genes related to cytokine signaling. Our results suggest that KDM5C restrains the expression of immune response genes in pDCs, and lack of this restraint leads to dysfunctional responses to further stimulation.

We have shown that KDM5C promotes mitochondrial gene expression in bone marrow monocytes (BMM) (49), similar to what we observe here in cDC1s. However, KDM5C-deficient BMM have significant decreases in mitochondrial function, which is contrary to our observation that KDM5C-deficient cDC1s display enhanced mitochondrial coupling (reduced proton leak) and elevated spare respiratory capacity. The differences in the role of KDM5C in these cell types is not clear but could be related to the availability and use of metabolic fuels in experimental conditions. The KDM5A-C *Drosophila* ortholog KDM5 (Lid) promotes the transcription of genes important for mitochondrial function (50) . However, KDM5 regulation of mitochondrial gene expression is mediated by the PHD3 domain, which is present in KDM5A/B but not KDM5C/D (50). How KDM5C then promotes transcription of these genes is not known. Positive regulation of gene expression by KDM5C has been linked to increased enhancer activity (by trimming H3K4me2/3 to H3K4me1) and co-activating gene expression (26,51). We found an enrichment of YY1 binding motifs, a transcription factor that promotes mitochondrial gene expression, suggesting that KDM5C function may be linked to this pathway. The implications of altered mitochondrial function for DC action are currently not clear; however, increased mitochondrial membrane potential to mass ratio has been associated with stress responses. Our results exemplify the importance of performing functional mitochondrial/metabolism assays to assess the consequences of changes in metabolic gene expression.

We found a strong IRF signature in genes dysregulated by cDC1 which likely is responsible for the increased inflammatory gene expression at steady state. IRF8 and IRF4 are key TFs involved in DC specification of cDC1 and cDC2, respectively. However, Kim *et al* show that IRF4 and IRF8 don't specifically produce cDC2 and cDC1, but rather the amount of IRF protein determines their identity(16). While this study was focused on IRF4 and 8, it is not clear if other IRFs could also contribute to the tally of IRF that determine DC specificity. Deletion of IRF8 in committed cDC1s causes the cells to acquire a cDC2-like transcriptional signature and functional properties (52). We find that KDM5C fine-tunes lineage-specific gene expression beyond IRF4 and 8. KDM5C-deficient cDC1 have increased expression of several cDC2-specific genes and a concomitant decreased expression of cDC1-specific games.

The significance of DC subset heterogeneity and how changes in heterogeneity alter inflammation and immunity is unclear. Because different subsets have specialized function, it is likely that the composition of the DC population impacts the efficacy and efficiency of immune responses. The balance of DC subsets varies among mouse strains, individuals, lifespan and during inflammation(5,53–56). Our findings demonstrate that there are factors such as KDM5C that influence the balance of DC subtypes, along with the ability of the DC population as a whole to respond to infection. How KDM5C impacts DC specification and whether its expression or function is regulated during infection, aging, or across strains warrants further examination. Additional investigation into how the balance of subsets

within the DC population affects immune responses will also provide further insight into how these cell types interact and work together to orchestrate a fully competent and efficient immune response in real world infection settings.

Experimental procedures

Mice

The following mouse strains were purchased from Jackson Laboratory and used for experiments and generating mouse lines used in this study; C57BL/6J (000664), *Ifnar*$^{-/-}$ (032045), *Zbtb*-Cre (028538), *Itgax*-Cre (008068), and Ly5.1 (002014). *Kdm5c*-fl/fl mice were a gift from the laboratory of Dr. Y. Shi and generated as described in (26,49,57). *Kdm5c*-fl/fl mice were crossed to *Itgax* and *Zbtb* Cre strains to produce the conditional knockout animals used in this work. Control mice were Kdm5cfl/fl-Cre negative. All mice were bred and maintained at Van Andel Research Institute Vivarium. All procedures involving mice were completed under approved IACUC protocols. All mice used were sex and age matched.

Tissue processing

Spleens were injected with HBSS (with Ca^{2+} and Mg^{2+}) containing 1 mg/mL of collagenase D and 10 µg/mL of DNase I (Roche) and incubated for 20 minutes at 37°C, followed by mashing and an additional 20 minute incubation at 37°C. The cell suspension was passed through a 70 µm cell strainer, then spun down at 300 x g for 5 minutes. The cell pellet was resuspended in 1 mL of RBC lysis buffer (155 mM NH_4Cl, 12mM $NaHCO_3$, and 0.125 mM EDTA) for 2 minutes, followed by addition of 4 mL of complete medium. The cells are spun down at 300 x g for 5 minutes and resuspended at the desired volume and buffer for downstream use.

Mouse models

pDC depletion

Mice were injected intraperitoneally with 250 µg of α-PDCA-1 or IgG2b antibody (Bio Xcell) in 100 µL of PBS every other day. Five days following the first injection, pDC depletion was confirmed in blood collected by retro-orbital bleed and stained for flow cytometry analysis. Following confirmation of pDC depletion, mice were sacrificed the next day and spleens were removed and processed to analyze by flow cytometry.

Bone marrow chimera

Ly5.1 mice were irradiated with two doses of 450 rad four hours apart. The next day, bone marrow from age-matched Ly5.1 mice (WT) and *Kdm5c*$^{\Delta Itgax}$ mice were extracted from the femurs and tibia. Cells were counted and resuspended to 25 x 10^6 non-RBCs per mL of PBS. 200 µL (5 x 10^6) of bone marrow cells from WT, *Kdm5c*$^{\Delta Itgax}$, or a 1:1 mix of WT and *Kdm5c*$^{\Delta Itgax}$ were intravenously injected per irradiated Ly5.1 mouse. Mice were kept on drinking water containing 0.17 mg/mL of enrofloxacin (pH 3.0) for 2 weeks. Spleen and bone marrow were collected and processed 7 weeks post-injection to examine by flow cytometry.

LCMV

Mice were infected with 2 x 10^5 PFU of LCMV Armstrong, which was diluted in PBS from a frozen stock and delivered intraperitoneally in a BSL2 biosafety cabinet. Infected mice were housed in a separate quarantine room and monitored for the indicated length of time until tissues were collected and processed.

Listeria

Attenuated *Listeria monocytogenes* expressing ovalbumin was grown in Tryptic Soy Broth containing streptomycin for 2-3 hours at 37°C and 250 rpm. Once an OD600 of 0.6 to 0.8 was reached, the bacteria were pelleted and diluted in PBS to a concentration of 2 x 10^7 CFU/mL. Listeria was administered intravenously at 2 x 10^6 CFU per mouse in a BSL2 biosafety cabinet. Mice were housed in a separate quarantine room and monitored for 7 days until tissues were harvested for immunophenotyping. For ex vivo analyses, splenocytes from mice infected for 7 days with LM-OVA were harvested and plated at 2x10^6/well in a 96-well non-tissue culture-treated plate. Cells were washed and stimulated in the presence of $OVA^{257-264}$ (1 µg/ml) (Anaspec), recombinant murine IL-2 200 U/ml (Peprotech) and 1x Brefeldin A

(BioLegend) at a final volume of 200 µl for 5.5 hours at 37°C in a humidified incubator. Following stimulation, cells were washed and processed for flow cytometry.

Flow cytometry
Samples were incubated with Fc block and eFluor 506 Fixable Viability Dye (ThermoFisher) in PBS, followed by an antibody cocktail prepared in wash buffer (PBS with 1% FBS, 1 mM EDTA, and 0.05% NaN_3). For intracellular staining, cells were fixed with IC fixation buffer (eBioscience/ThermoFisher) for 30 minutes following surface staining, permeabilized using Permeabilization Buffer (eBioscience/ThermoFisher) and incubated for at least one hour with antibodies targeting intracellular proteins. Samples were acquired on the Cytek Aurora spectral cytometer and data analyzed using FlowJo v10. For mitochondrial staining, cells were plated and warmed to 37°C before staining. Mitochondrial dyes MitoSpy Green (BioLegend, 424806) and TMRM (ThermoFisher Scientific, T668) were prepared at 2x in HBSS, warmed, and added 1:1 to plated cells. Plates were incubated at 37°C for 20 minutes, washed, and surfaced stained. Cell sorting was performed on a Symphony S6 (BD Biosciences) or Moflo Astrios EQ Sorter (Beckman Coulter).

IFN-a enzyme-linked immunosorbent assay (ELISA)
$Ly6C^+$ and $Ly6C^-$ pDCs that are PDCA-$1^+B220^+CD11b^-CD11c^{int}$ were sorted from *Kdm5c*$^{\Delta Itgax}$ or control spleens and samples were pooled together for biological replicates of 15,000 cells per well. Cells were resuspended in 100 µL of complete medium (RPMI 1640 and 10% FBS, 2 mM L-glutamine, 100 U/mL penicillin/streptomycin, 0.01% β-mercaptoethanol) prior to plating, and 2X treatment was added to each well in 100 µL of complete medium. Cells were treated with CpG ODN 1585 to stimulate IFN responses (Invivogen; catalog # tlr-kit9m). After treatment for 18 hours, supernatant was collected and IFN-α measured by ELISA according to manufacturer's instructions (Invitrogen; catalog # BMS6027)

In vitro DC differentiation with FLT3L
Mouse tibia and femur were washed with 70 % EtOH followed by PBS, and bone marrow was extracted. 2 x 10^5 bone marrow cells (not counting RBC) were seeded per well in a 96-well plate in RPMI-1640 containing 10% FBS (NuSerum), 2 mM L-glutamine, 100 U/mL of penicillin/streptomycin, 0.55 µM β-mercaptoethanol, and 100 ng/mL FLT3L (Peprotech), with or without 50 U/mL IFN-β (PBL Interferon Source). After 3 days, 2.5 x 10^5 mitomycin-treated OP9-DL1 cells (kindly gifted by Boris Reizis laboratory) were seeded in a tissue culture-treated 96-well plate (58). The OP9-DL1 cells were allowed to settle for approximately 2 hours prior to transferring over the bone marrow cells with replenished media with 100 ng/mL FLT3L with or without IFN-β as before. After 4 additional days, cells were stained to analyze by flow cytometry.

Western blot
Protein lysates from FACS-sorted cDCs from control and *Kdm5c*$^{\Delta Itgax}$ or *Kdm5c*$^{\Delta Zbtb46}$ spleens were prepared using CHAPS lysis buffer (Cell Signaling, 9852S) with protease inhibitors (Roche, 11836170001), quantified with Pierce 660 nm Protein Assay Reagent (ThermoFisher Scientific; 1861426), and mixed with Laemmli sample buffer (BioWorld 10570021). 25 µg of protein per sample was loaded into 4-20% pre-cast polyacrylamide gels (Bio-Rad) and proteins were transferred to methanol-activated polyvinylidine fluoride membranes. Membranes were blocked for 1 hour using 5% milk in Tris-buffer saline (TBS) containing 0.1% Tween-20 (TBS-T), followed by overnight incubation at 4°C with anti-KDM5C antibody (1:1000; Abcam; Ab194288) in 5% milk in TBS-T, or 1 hour at room temperature with anti-β-actin antibody (1:1000; Cell Signaling; 4967S) in 5% bovine serum albumin (BSA) in TBS-T. Following washes with TBS-T, membranes were incubated with anti-rabbit horseradish peroxidase-linked antibody (Cell Signaling; 7074S) at a dilution of 1:4000 in 5% milk for 2 hours at room temperature for KDM5C, or 1:10 000 in 5% milk for 1 hour at room temperature for β-actin. Blots were developed by enhanced chemiluminescence using SuperSignal West Dura Extended Duration Substrate (ThermoFisher Scientific; 34075) and Bio-Rad ChemiDoc MP Imaging System.

Metabolic assay
Several metabolic parameters were assessed in sorted cDC1 using the XF Cell Mito Stress Test and Seahorse XFe96 Analyzer (Agilent). cDC1s were labeled with PE-XCR1 antibody for positive selection using magnet after pan-DC enrichment (Miltenyi). The cell plate was coated with poly-D-lysine, then 200,000 cells were seeded per well in XF RPMI medium containing 10 mM glucose and 2 mM L-glutamine, with pH adjusted to 7.4. The plate was then incubated at 37°C in a non-CO2 incubator for 1 hour prior to the assay. Cells were sequentially treated with oligomycin (1.5 µM), FCCP (3 µM), and rotenone/antimycin A (0.5 µM), and oxygen consumption rate (OCR) was measured. At the end of each assay, cells were stained with Hoescht stain (20 µM; ThermoFisher Scientific) for 15 minutes at 37°C, then imaged using a Cytation imaging reader (Cytek) to count cells. OCR measurements were normalized by cell number.

ATAC-seq
Libraries for ATAC-seq were prepared from nuclei of 25,000 sorted cells using the Omni-ATAC protocol in which mitochondrial DNA is depleted, enabling increased read-depth on genomic DNA(59,60). Transposition and amplification reactions were performed using the Nextera XT DNA Library preparation kit (Illumina cat# 15032354) along with IDT for Illumina adapters. Libraries were size-selected using Ampure XP beads (cat# A63881) and sequenced 50 bp, paired-end on an Illumina NovaSeq6000 sequencer. The data were trimmed using TrimGalore v0.6.0 (https://github.com/FelixKrueger/TrimGalore) to eliminate low-quality bases, and subsequently aligned to the mouse reference genome GRCm38 using bwa mem v0.7.17(61) . Duplicates were marked using SAMBLASTER v0.1.24 (62) , and low-quality bases filtered using SAMtools v1.9 (63) . The bamCoverage tool in deepTools v3.4.3 (64) was utilized to generate BigWig files, excluding regions blacklisted in the ENCODE v2 blacklist(65). Furthermore, deepTools was employed to create heatmaps that visualize the distribution of chromatin accessibility levels surrounding gene regions. Differential accessibility analyses were performed using diffbind version 3.8.4 (66).

RNA-seq
15,000 cells were FACS sorted into 1.5ml tubes containing 350ul lysis buffer. (Norgen Biotek buffer RL) RNA was extracted using Single Cell RNA Purification kit from Norgen Biotek (cat# 51800) and quantified using qubit HS RNA Assay kit (cat# Q32852). RNA libraries were generated using Takara SMARTer Stranded total RNA-seq Kit v3 (cat# 634487) and sequenced 50 bp, paired-end on an Illumina NovaSeq6000 sequencer. Reads were aligned to the mm10 genome and ERCC sequences using Takara's CogentAP v1.5, specifying the 'Strnd_UMI' kit configuration. The deduplicated (via UMIs) counts were imported into R v4.1.0 for further analysis. Genes with >2 counts in at least 2 samples were retained. Differential expression for pairwise contrasts was tested using DESeq2 v1.32.0(67) with a significance cutoff of 0.1 FDR; a model design of '~ Group' was used, where Group represents unique combinations of genotype, treatment and cell type. Log fold changes were shrunken using the 'lfcShrink' function, with the parameter, "type='ashr'" (68) and used to rank genes for GSEA analysis using clusterProfiler v4.0.5 (69)).

CUT&RUN
Libraries for CUT&RUN-seq were prepared from 25,000 sorted cells(70). Transposition and amplification reactions were performed using the Nextera DNA Library preparation kit (Illumina) and sequenced 50 bp, paired-end on an Illumina NovaSeq6000 sequencer. Reads were trimmed using TrimGalore v0.6.0 with default parameters and aligned to the mm10 genome and decoy sequences, including viral sequences and cfMeDIP-seq spike-in sequences, (71,72)using bwa mem v0.7.17 (61). PCR duplicates were marked using SAMBLASTER v0.1.24 (62). Only high-confidence and properly-paired alignments were retained using samtools view with parameters, "-q 30 -f 2 -F 2828" (v1.9)(73). For peak calling, duplicate alignments were removed and processed with MACS2 v2.2.7.1(74) with the

parameters, "-f BAMPE -g mm --keep-dup 'all'". Called peaks were filtered to remove ENCODE blacklist v2 regions(65). Bigwig files for visualization was produced using DeepTools v3.4.3(64); bamCoverage was run with the parameters, "--binSize 10 --extendReads --normalizeUsing 'CPM' --samFlagExclude 1024 --samFlagInclude 64". Bigwig files were combined across replicates by finding the mean using WiggleTools v1.2.11(75) and wigToBigWig from UCSC tools. Coverage heatmaps were generated using Deeptools v3.4.3.

Differential PTM was tested using DiffBind v3.2.7(76). For read counting, 'dba.count' was run with the parameters, 'summits=200, bUseSummarizeOverlaps = TRUE', with SummarizeOverlaps configured to paired-end mode. For sample normalization, 'dba.normalize' was run with the parameters, 'normalize = DBA_NORM_NATIVE, background = TRUE'. The 'dba.analyze' step was run with the parameters, 'bBlacklist=FALSE, bGreylist=FALSE'. Pairwise contrasts between different combinations of genotype and cell type were tested using an FDR cutoff of 0.1. Significant peaks were annotated to their nearest gene using ChIPSeeker v1.28.3(77), considering -3000 to +500 as the promoter region. For pathway enrichment analysis, peaks labeled as "Distal Intergenic" were removed and peaks were separated into up and down-regulated. Overlapping genes were tested using hypergeometric tests as implemented in clusterProfiler v4.0.5.

Heatmaps

Heatmaps were generated using pheatmap version 1.0.12 package in R (version 4.4.2).

HOMER Analysis

The findMotifs.pl script in HOMER(78) version 4.11 was utilized to identify transcription factor binding sites (TFBS) using gene lists obtained from transcriptomics differential expression analyses. The search criteria for TFBS included lengths ranging from 8 to 10 bases, and their locations were restricted to within 2000 bases upstream and 100 bases downstream of the transcription start site (TSS).

Figure legends

Figure 1 - KDM5C regulates pDC heterogeneity. (**A**) The proportions and cell counts of splenic Ly6C$^+$ pDCs and Ly6C$^-$ pDCs from female control and *Kdm5c*$^{\Delta Itgax}$ mice were determined by flow cytometry. Numbers above gates in representative FACS plots (left) indicate frequencies of Ly6C$^+$ pDCs or Ly6C$^-$ pDCs as a percentage of the parent population (Lin(B220)$^+$SiglecH$^+$CD11c^{int}CD11b$^-$). (**B**) Geometric mean fluorescence intensity (MFI) of activation markers CD80, MHCII, PD-L1, CD86 and CD40 expressed by Ly6C$^+$ (red bars) and Ly6C$^-$ pDCs (orange bars). (**C**) Dot plots of RNA-seq analysis comparing Ly6C$^+$ and Ly6C$^-$ pDCs with Reactome Pathway Analysis and GSEA of Biological Processes (left); heatmap of cell cycle genes (right). (**D**) Proportions of CD4$^+$ and CD4$^-$ cells as a percentage of Ly6C$^+$ pDCs (dark red bars) or Ly6C$^-$ pDCs (orange bars) (left) and percentage of Ly6C$^+$ or Ly6C$^-$ pDCs of Lin(B220)$^+$SiglecH$^+$CD11c^{int}CD11b$^-$ cells in bone marrow (BM) and spleen (right). (**E**) Proportions of splenic pDCs at steady state and 1 day post infection with LCMV Armstrong (LCMV-ARM). (**F**) Proportion of Ly6C$^+$CD11c$^+$B220$^+$MHCII$^-$ pDCs as a percentage of live cells following differentiation of bone marrow with FLT3L in the presence of IFN-β (50 U/mL). (**G**) IFN-α production by sorted splenic Ly6C$^+$ and Ly6C$^-$ pDCs stimulated with TLR9 ligand CpG ODN 1585 for 18 hours, measured by ELISA and expressed as fold change relative to stimulated control Ly6C$^+$ pDCs. (**H**) Percentages of Ly6C$^+$ and Ly6C$^-$ pDCs of total cells following CpG stimulation of sorted Ly6C$^-$ pDCs. (**I**) Frequencies and cell counts of splenic Ly6C$^+$ pDCs and Ly6C$^-$ pDCs from WT and *Ifnar1*$^{-/-}$ mice. Numbers above gates in representative FACS plots indicate percentages of Ly6C$^+$ pDCs or Ly6C$^-$ pDCs of live cells. Each symbol from (**A, B, H**) represents an individual mouse. Data are (**A**) pooled from 2 experiments (mean and s.e.m. of 10 to 11 mice per group), (**B**) one experiment representative of three experiments (mean and s.e.m. of 4 mice per group), (**F**) one experiment representative of three experiments (mean and s.d. of four replicates

per group), (**G, H**) one experiment (mean and s.e.m. of 4 biological replicates per group), (**I**) pooled from three experiments (mean and s.e.m. of 13 to 14 mice per group). Statistical significance was determined by unpaired *t*-test. * $p < 0.05$, ** $p < 0.01$, *** $p < 0.001$, **** $p < 0.0001$

Figure 2 - KDM5C alters transcriptional profiles and impairs type I IFN production by pDCs. (**A**) Geometric MFI of activation markers CD80, MHCII, PD-L1, CD86, and CD40 of Ly6C$^+$ and Ly6C$^-$ pDCs from control or *Kdm5c$^{\Delta Itgax}$* mice. (**B**) Bone marrow cells that were either a 1:1 mixture of CD45.1$^+$ WT and CD45.2$^+$ *Kdm5c$^{\Delta Itgax}$* cells or CD45.2$^+$ *Kdm5c$^{\Delta Itgax}$* cells alone were transferred into lethally irradiated CD45.1$^+$ WT mice. Proportions of splenic cDC subsets derived from CD45.1$^+$ WT and CD45.2$^+$ *Kdm5c$^{\Delta Itgax}$* cells and geometric MFI of MHCII and CD40 were determined 7 weeks post-injection. (**C**) Volcano plots of RNA-seq of control and *Kdm5c$^{\Delta Itgax}$* Ly6C$^-$ and Ly6C$^+$ pDCs with or without LCMV infection (20 hours). Red data points indicate differential expression. (**D**) Significantly different Pathway and GSEA analysis of control and Kdm5c$^{\Delta Itgax}$ Ly6C$^+$ pDCs with LCMV infection. (**E**) Heat maps of genes from select pathways from (**D**); BP pathway negative regulation of immune system (left) and KEGG pathway antigen processing and presentation (right). (**F**) IFN-α production by sorted splenic Ly6C$^+$ and Ly6C$^-$ pDCs from control and *Kdm5c$^{\Delta Itgax}$* mice that were stimulated with TLR9 ligand CpG ODN 1585 for 18 hours, measured by ELISA and expressed as fold change relative to stimulated control Ly6C$^+$ pDCs. Data are of (**A**) one experiment representative of > three experiments (mean and s.e.m. of 7 mice per group), (**B**) pooled from two experiments (cell proportions; mean and s.e.m. of 18 mice from mixed donor group and 9 mice from *Kdm5c$^{\Delta Itgax}$* donor alone) or one experiment representative of two experiments (activation markers; mean and s.e.m. of 8 mice for mixed donor group and 5 mice for *Kdm5c$^{\Delta Itgax}$* donor alone), (**F**) pooled averages from two to three experiments (mean and s.e.m. of 2 to 3 per group, with each data point representing an individual experiment). Statistical significance was determined by (**A**) unpaired *t*-test, or (**B, F**) one-way ANOVA. * $p < 0.05$, ** $p < 0.01$, *** $p < 0.001$, **** $p < 0.0001$

Figure 3 - KDM5C regulates cDC heterogeneity. In female control and *Kdm5c$^{\Delta Itgax}$* mice, the cell counts and frequencies of (**A**) splenic XCR1$^+$ cDC1s, XCR1$^-$CD172a$^-$ merocytic DCs (top), CLEC12A$^-$ cDC2A, and CLEC12A$^+$ cDC2B (bottom) were determined by flow cytometry. Numbers next to gates in representative FACS plots (left) indicate percentages of cDC1, cDC2, or merocytic DCs as a percentage of total cDCs (Lin$^-$MHCII$^+$CD11c$^+$CD26$^+$) or cDC2A or cDC2B as a percentage of CD172a$^+$ cDC2s. (**B**) As in (**A**), cDC subset proportions were determined by flow cytometry in *Kdm5c$^{\Delta Zbtb46}$*. Proportions of cDC1, cDC2A, and cDC2B of (**C**) mice administered α-IgG2b or α-PDCA1 to deplete pDCs, or **(D)** WT or *Ifnar-/-* mice. (**G**) Bone marrow cells that were either a 1:1 mixture of CD45.1$^+$ WT and CD45.2$^+$ *Kdm5c$^{\Delta Itgax}$* cells or CD45.2$^+$ *Kdm5c$^{\Delta Itgax}$* cells alone were transferred into lethally irradiated CD45.1$^+$ WT mice. Proportions of splenic cDC subsets derived from CD45.1$^+$ WT and CD45.2$^+$ *Kdm5c$^{\Delta Itgax}$* cells as a percentage of total cDCs were determined 7 weeks post-injection. Data are pooled from (**A**) two experiments (mean and s.e.m. of 10 to 11 mice per group), (**B**) two experiments (mean and s.e.m. of 7 to 8 mice per group), (**C**) two experiments (mean and s.e.m. of 10 mice per group), (**D**) three experiments (mean and s.e.m. of 14 mice per group), and (**E**) two experiments (mean and s.e.m. of 18 mice from mixed donor group and 9 mice from *Kdm5c$^{\Delta Itgax}$* donor alone). Statistical significance was determined by (**A-D**) unpaired *t*-test or (**E**) one-way ANOVA. * $p < 0.05$, ** $p < 0.01$, *** $p < 0.001$, **** $p < 0.0001$

Figure 4 - Disruption of epigenetic and transcriptional programming in cDC1 at homeostasis in the absence of KDM5C. RNA-seq analyses of control and KDM5C-deficient cDC1. Pathway analyses (**A**) and heatmaps (**B**) of differentially expressed genes. (**C**) HOMER analyses of promoters of genes upregulated in the absence of KDM5C. (**D**) Heatmap of Irf genes. (**E**) Heatmaps of H3K4me3 (CUT&RUN) segregated by direction of differential expression. (**F**) Pathway analysis of genes with differentially methylated regions. (**G**) IGV tracks showing H3K4me3, H3K27Ac, Accessibility (ATAC-seq) and RNA expression (RNA-Seq). Data is shown is combined from 3 biological replicates of each genotype.

Figure 5 - KDM5C regulates OXPHOS gene expression and mitochondrial function in cDC1. (**A**) Heat map of differentially expressed genes encoding factors from KEGG OXPHOS pathway by splenic cDC1 from control and *Kdm5c*$^{\Delta Itgax}$ mice. (**B**) Geometric MFI of MitoSpy Green (mitochondrial mass) and TMRM (mitochondrial membrane potential), and ratio of mitochondrial membrane potential to mass. (**C**) Oxygen consumption rate (OCR) measured over time of sorted control and *Kdm5c*$^{\Delta Itgax}$ cDC1 sequentially treated by oligomycin, FCCP, and rotenone/antimycin A (top). From this profile, several parameters were calculated (bottom): basal respiration (OCR of cells without drug treatment), spare respiratory capacity (SRC; maximal respiration minus basal respiration), maximal respiration (OCR following FCCP treatment), and proton leak (OCR following oligomycin treatment minus OCR following rotenone/antimycin A treatment). (**D**) Heatmap of H3K4me3 of genes shown in A. (**E**) IGV tracks showing H3K4me3, H3K27Ac, Accessibility (ATAC-seq) and RNA expression (RNA-Seq). Data is shown is combined from 3 biological replicates. Data are of one experiment representative of (**B**) two experiments (mean and s.e.m. of 3 WT and 6 *Kdm5c*$^{\Delta Itgax}$ mice), (**C**) two experiments (mean and s.e.m. of 3 replicates).

Figure 6 - Alterations in DC lineage-specific gene expression and function in the absence of KDM5C. (**A**) Heat map of gene expression of markers specific to cDC subsets by cDC1, cDC2A, and cDC2B sorted from control and *Kdm5c*$^{\Delta Itgax}$ splenocytes. (**B**) IGV tracks showing H3K4me3, H3K27Ac, Accessibility (ATAC-seq) and RNA expression (RNA-Seq). Data is shown is combined from 3 biological replicates. (**C**) Geometric MFI of IRF8 in control and *Kdm5c*$^{\Delta Itgax}$ cDC1. Control and *Kdm5c*$^{\Delta Itgax}$ mice were infected with *Listeria monocytogenes* expressing ovalbumin (LmOVA) for 7 days, and assessed the frequencies of (**D**) CD44^{+} (top) and CD11a^{+}CD49d^{+} (bottom) of CD4^{+} T cells (**E**) ovalbumin-specific (tetramer^{+}) cells of CD8^{+} T cells, and (**F**) IFN-γ^{+} of CD8^{+} T cells (top) and IFN-γ^{+}TNF-α^{+} polyfunctional cells of CD8^{+}CD44^{+} T cells (bottom). Data from (**C**) are of one experiment representative of three experiments (mean and s.e.m. of 5 mice per group), (**D-F**) are pooled from two experiments (mean and s.e.m. of 8 control and 11 *Kdm5c*$^{\Delta Itgax}$ mice). Statistical significance in (**C-F**) were determined by unpaired *t*-test.

Supplementary figure legends

cDC/pDC

Marker	**Manufacturer**	**Product #**	**Clone**	**Fluorophore**	**Dilution**
CD86	BD Biosciences	564199	GL1	BUV395	300
CD80	BD Biosciences	741272	16-10A1	BUV563	300
CD11c	BD Biosciences	749039	N418 (RUO)	BUV737	300
CLEC12A	BD Biosciences	564795	5D3/CD371	BV421	200
PDCA1 CD317	Biolegend	127018	927	PB	300
Viability	eBioscience	65-2860-40		e506	1000
CD11b	Biolegend	101233	M1/70	BV570	300

MHC II I-A/I-E	biolegend	107639	M5/114.15.2	BV605	1000
XCR1	Biolegend	148220	ZET	BV650	300
Ly6C	Biolegend	128037	HK1.4	BV711	1500
CD40	eBioscience	78-0401-82	1C10	SB780	300
CX3CR1	Biolegend	149006	SA011F11	PE	300
F4/80	Biolegend	123146	BM8	PE/Dazzle	300
PD-L1 CD274	Biolegend	124314	10F.9G2	PE Cy7	400
CD64	Biolegend	139308	X54-5/7.1	PercpCy5.5	100
CD26	Biolegend	137807	H194-112	APC	200
CD172a	Biolegend	144022	P84	AF700	200
Siglec H	Miltenyi	130-112-299	REA819	APC vio770	300
Ly6G (1A8)	eBioscience	11-9668-82	1AB-Ly6g	FITC	500
B220	eBioscience	11-0452-82	RA3-6B2	FITC	500
CD3	eBioscience	11-0032-82	17A2	FITC	300
CD19	eBioscience	11-0193-85	eBio1D3(1D3)	FITC	300
NK1.1	Biolegend	11-5941-82	PK136	FITC	300

Sorting panel

Marker	**Manufacturer**	**Product #**	**Clone**	**Fluorophore**	**Dilution**
MHCII	Biolegend	107639	M5/114.15.2	BV605	600
CLEC12A	Biolegend	143405	5D3/CLEC12A	APC	200
XCR1	Biolegend	148224	ZET	APCCy7	200
CD3	eBioscience	11-0032-82	17A2	FITC	200
CD19	eBioscience	11-0193-85	eBio1D3(1D3)	FITC	200
NK1.1	Biolegend	11-5941-82	PK136	FITC	200

Ly6G	eBioscience	11-9668-82	1AB-Ly6g	FITC	200
CD64	Biolegend	139316	X54-5/7.1	FITC	200
F480	Biolegend	123146	BM8	PE-Dazzle594	200
CD11b	eBioscience	45-0112-80	M1/70	Percp-Cy5.5	200
CD11c	eBioscience	25-0114-82	N418	Pe-Cy7	300
CD172a	Biolegend	144022	P84	AF700	200
PDAC1	Biolegend	127023	927	BV421	200
B220	Biolegend	103241	RA3-6B2	BV650	200
Ly6C	eBioscience	12-5932-82	HK1.4	PE	200
viability				DAPI	500

Tetramer panel

Marker	**Manufacturer**	**Product #**	**Clone**	**Fluorophore**	**Dilution**
CD62L	BD Biosciences	740218	MEL-14	BUV395	300
CD4	BD Biosciences	741050	RM4-5	BUV496	300
KLRG1	BD Biosciences	741586	2F1	BUV661	300
CD8a	BD Biosciences	612898	53-6.7	BUV805	300
CD223	eBioscience	48-2231-80	eBioC9B7W(C9B7W)	e450	300
PD-1	Biolegend	135219	29F.1A12	BV605	300
CD44	Biolegend	103049	1M7	BV650	600
CD127	Biolegend	135037	A7R34	BV785	100
CD3e	eBioscience	45-0031-82	145-2C11	PerCP Cy5.5	200
B220	eBioscience	11-0452-82	RA3-6B2	FITC	300
Ly6G	eBioscience	11-9668-82	1AB-Ly6g	FITC	300
NK1.1	Biolegend	108705	PK136	FITC	300

CD19	eBioscience	11-0193-85	eBio1D3(1D3)	FITC	300
OVATET	Baylor College of Medicine	108708	Tetramer	PE	250
CD49d	Biolegend	103626	R1-2	PE Dazzle	600
CD11a	Biolegend	101122	M17/4	PECY7	800
CD25	eBioscience	17-0251-82	PC61.5	APC	300
Viability	eBioscience	65-0865-14		APC e780	1500

Restim panel

Marker	**Manufacturer**	**Product #**	**Clone**	**Fluorophore**	**Dilution**
KLRG1	eBioscience	58-5893-80	2F1	AF532	300
CX3CR1	Biolegend	149036	SA011F11	AF700	100
CD8A	eBioscience	47-0081-82	53-6.7	APC Fire 750	300
CD44	BD Biosciences	741921	IM7	BUV 805	300
CD62L	Biolegend	740218	MEL-14	BUV 395	300
CD69	BD Biosciences	741063	H1.2F3	BUV 496	100
CD127	Biolegend	135037	A7R34	BV785	100
LY108	Biolegend	134608	330-AJ	Pac Blue	100
Viability	Thermo Fisher	65-2860-40		e506	500
TIM3	Biolegend	119727	RMT3-23	BV711	100
CD279	BD Biosciences	749306	RMPI-30	BUV 737	100
CD4	eBioscience	15-0042-83	RM4-5	PE-CY5	300
IFNg	eBioscience	17-7311-82	XMG1.2	FITC	100
TNFa	eBioscience	25-7321-82	MP6-X1222	PE-Cy7	200
Tox	eBioscience	46-4875-82	Dan11mag	PE	100
TCF1	eBioscience	6709S	C63D9	AF647	100
GZMB	Biolegend	372216	QA16A02	PE-Dazzle	100
TBET	Biolegend	644817	4B10	BV605	100

References

1. Brown CC, Gudjonson H, Pritykin Y, Deep D, Lavallée V-P, Mendoza A, et al. Transcriptional Basis of Mouse and Human Dendritic Cell Heterogeneity. Cell. 2019 Oct 31;179(4):846-863.e24.

2. Naik SH, Sathe P, Park H-Y, Metcalf D, Proietto AI, Dakic A, et al. Development of plasmacytoid and conventional dendritic cell subtypes from single precursor cells derived in vitro and in vivo. Nat Immunol. 2007 Nov;8(11):1217–26.

3. Schlitzer A, Sivakamasundari V, Chen J, Sumatoh HRB, Schreuder J, Lum J, et al. Identification of cDC1- and cDC2-committed DC progenitors reveals early lineage priming at the common DC progenitor stage in the bone marrow. Nat Immunol. 2015 Jul;16(7):718–28.

4. Rodrigues PF, Alberti-Servera L, Eremin A, Grajales-Reyes GE, Ivanek R, Tussiwand R. Distinct progenitor lineages contribute to the heterogeneity of plasmacytoid dendritic cells. Nat Immunol.

2018 Jul;19(7):711–22.

5. Guilliams M, Dutertre C-A, Scott CL, McGovern N, Sichien D, Chakarov S, et al. Unsupervised High-Dimensional Analysis Aligns Dendritic Cells across Tissues and Species. Immunity. 2016 Sep 20;45(3):669–84.

6. Musumeci A, Lutz K, Winheim E, Krug AB. What Makes a pDC: Recent Advances in Understanding Plasmacytoid DC Development and Heterogeneity. Front Immunol. 2019 May 29;10:1222.

7. Villani A-C, Satija R, Reynolds G, Sarkizova S, Shekhar K, Fletcher J, et al. Single-cell RNA-seq reveals new types of human blood dendritic cells, monocytes, and progenitors. Science [Internet]. 2017 Apr 21;356(6335). Available from: http://dx.doi.org/10.1126/science.aah4573

8. Zhang H, Gregorio JD, Iwahori T, Zhang X, Choi O, Tolentino LL, et al. A distinct subset of plasmacytoid dendritic cells induces activation and differentiation of B and T lymphocytes. Proc Natl Acad Sci U S A. 2017 Feb 21;114(8):1988–93.

9. Alcántara-Hernández M, Leylek R, Wagar LE, Engleman EG, Keler T, Marinkovich MP, et al. High-Dimensional Phenotypic Mapping of Human Dendritic Cells Reveals Interindividual Variation and Tissue Specialization. Immunity. 2017 Dec 19;47(6):1037-1050.e6.

10. Dress RJ, Dutertre C-A, Giladi A, Schlitzer A, Low I, Shadan NB, et al. Plasmacytoid dendritic cells develop from Ly6D lymphoid progenitors distinct from the myeloid lineage [Internet]. Vol. 20, Nature Immunology. 2019. p. 852–64. Available from: http://dx.doi.org/10.1038/s41590-019-0420-3

11. Feng J, Pucella JN, Jang G, Alcántara-Hernández M, Upadhaya S, Adams NM, et al. Clonal lineage tracing reveals shared origin of conventional and plasmacytoid dendritic cells. Immunity. 2022 Mar 8;55(3):405-422.e11.

12. Rodrigues PF, Kouklas A, Cvijetic G, Bouladoux N, Mitrovic M, Desai JV, et al. pDC-like cells are pre-DC2 and require KLF4 to control homeostatic CD4 T cells. Science Immunology. 2023;8(80):eadd4132.

13. Sichien D, Scott CL, Martens L, Vanderkerken M, Van Gassen S, Plantinga M, et al. IRF8 Transcription Factor Controls Survival and Function of Terminally Differentiated Conventional and Plasmacytoid Dendritic Cells, Respectively. Immunity. 2016 Sep 20;45(3):626–40.

14. Suzuki S, Honma K, Matsuyama T, Suzuki K, Toriyama K, Akitoyo I, et al. Critical roles of interferon regulatory factor 4 in CD11bhighCD8alpha- dendritic cell development. Proc Natl Acad Sci U S A. 2004 Jun 15;101(24):8981–6.

15. Satpathy AT, Briseño CG, Lee JS, Ng D, Manieri NA, Kc W, et al. Notch2-dependent classical dendritic cells orchestrate intestinal immunity to attaching-and-effacing bacterial pathogens. Nat Immunol. 2013 Sep;14(9):937–48.

16. Kim S, Bagadia P, Anderson DA 3rd, Liu T-T, Huang X, Theisen DJ, et al. High Amount of Transcription Factor IRF8 Engages AP1-IRF Composite Elements in Enhancers to Direct Type 1 Conventional Dendritic Cell Identity. Immunity. 2021 Jul 13;54(7):1622.

17. Anderson DA 3rd, Murphy KM, Briseño CG. Development, Diversity, and Function of Dendritic Cells in Mouse and Human. Cold Spring Harb Perspect Biol [Internet]. 2018 Nov 1;10(11).

Available from: http://dx.doi.org/10.1101/cshperspect.a028613

18. Murphy TL, Grajales-Reyes GE, Wu X, Tussiwand R, Briseño CG, Iwata A, et al. Transcriptional control of dendritic cell development. Annu Rev Immunol. 2016 May 20;34:93–119.

19. Nutt SL, Chopin M. Transcriptional Networks Driving Dendritic Cell Differentiation and Function. Immunity. 2020 Jun 16;52(6):942–56.

20. Lukowski SW, Rødahl I, Kelly S, Yu M, Gotley J, Zhou C, et al. Absence of Batf3 reveals a new dimension of cell state heterogeneity within conventional dendritic cells. iScience. 2021 May 21;24(5):102402.

21. Grajales-Reyes GE, Iwata A, Albring J, Wu X, Tussiwand R, Kc W, et al. Batf3 maintains autoactivation of Irf8 for commitment of a CD8α(+) conventional DC clonogenic progenitor. Nat Immunol. 2015 Jul;16(7):708–17.

22. Bagadia P, Huang X, Liu T-T, Durai V, Grajales-Reyes GE, Nitschké M, et al. An Nfil3-Zeb2-Id2 pathway imposes Irf8 enhancer switching during cDC1 development. Nat Immunol. 2019 Sep;20(9):1174–85.

23. Boukhaled GM, Cordeiro B, Deblois G, Dimitrov V, Bailey SD, Holowka T, et al. The Transcriptional Repressor Polycomb Group Factor 6, PCGF6, Negatively Regulates Dendritic Cell Activation and Promotes Quiescence. Cell Rep. 2016 Aug 16;16(7):1829–37.

24. Iwase S, Lan F, Bayliss P, de la Torre-Ubieta L, Huarte M, Qi HH, et al. The X-linked mental retardation gene SMCX/JARID1C defines a family of histone H3 lysine 4 demethylases. Cell. 2007 Mar 23;128(6):1077–88.

25. Shen H-F, Zhang W-J, Huang Y, He Y-H, Hu G-S, Wang L, et al. The Dual Function of KDM5C in Both Gene Transcriptional Activation and Repression Promotes Breast Cancer Cell Growth and Tumorigenesis. Adv Sci. 2021 May;8(9):2004635.

26. Outchkourov NS, Muiño JM, Kaufmann K, van Ijcken WFJ, Groot Koerkamp MJ, van Leenen D, et al. Balancing of histone H3K4 methylation states by the Kdm5c/SMCX histone demethylase modulates promoter and enhancer function. Cell Rep. 2013 Apr 25;3(4):1071–9.

27. Greenfield A, Carrel L, Pennisi D, Philippe C, Quaderi N, Siggers P, et al. The UTX gene escapes X inactivation in mice and humans. Hum Mol Genet. 1998 Apr;7(4):737–42.

28. Wu L, Cao J, Cai WL, Lang SM, Horton JR, Jansen DJ, et al. KDM5 histone demethylases repress immune response via suppression of STING. PLoS Biol. 2018 Aug;16(8):e2006134.

29. Chen K, Luan X, Liu Q, Wang J, Chang X, Snijders AM, et al. Drosophila Histone Demethylase KDM5 Regulates Social Behavior through Immune Control and Gut Microbiota Maintenance. Cell Host Microbe. 2019 Apr 10;25(4):537-552.e8.

30. Tricarico R, Nicolas E, Hall MJ, Golemis EA. X- and Y-Linked Chromatin-Modifying Genes as Regulators of Sex-Specific Cancer Incidence and Prognosis. Clin Cancer Res. 2020 Nov 1;26(21):5567–78.

31. Doss PMIA, Umair M, Baillargeon J, Fazazi R, Fudge N, Akbar I, et al. Male sex chromosomal complement exacerbates the pathogenicity of Th17 cells in a chronic model of central nervous system autoimmunity. Cell Rep. 2021 Mar 9;34(10):108833.

32. Zhan Y, Chow KV, Soo P, Xu Z, Brady JL, Lawlor KE, et al. Plasmacytoid dendritic cells are short-lived: reappraising the influence of migration, genetic factors and activation on estimation of lifespan. Sci Rep. 2016 Apr 26;6:25060.

33. Reizis B. Plasmacytoid Dendritic Cells: Development, Regulation, and Function. Immunity. 2019 Jan 15;50(1):37–50.

34. Audiger C, Fois A, Thomas AL, Janssen E, Pelletier M, Lesage S. Merocytic Dendritic Cells Compose a Conventional Dendritic Cell Subset with Low Metabolic Activity. J Immunol. 2020 Jul 1;205(1):121–32.

35. Lewis KL, Caton ML, Bogunovic M, Greter M, Grajkowska LT, Ng D, et al. Notch2 receptor signaling controls functional differentiation of dendritic cells in the spleen and intestine. Immunity. 2011 Nov 23;35(5):780–91.

36. Abram CL, Roberge GL, Hu Y, Lowell CA. Comparative analysis of the efficiency and specificity of myeloid-Cre deleting strains using ROSA-EYFP reporter mice. J Immunol Methods. 2014 Jun;408:89–100.

37. Krawczyk CM, Holowka T, Sun J, Blagih J, Amiel E, DeBerardinis RJ, et al. Toll-like receptor-induced changes in glycolytic metabolism regulate dendritic cell activation. Blood. 2010 Jun 10;115(23):4742–9.

38. Guak H, Al Habyan S, Ma EH, Aldossary H, Al-Masri M, Won SY, et al. Glycolytic metabolism is essential for CCR7 oligomerization and dendritic cell migration [Internet]. Vol. 9, Nature Communications. 2018. Available from: http://dx.doi.org/10.1038/s41467-018-04804-6

39. Guak H, Sheldon RD, Beddows I, Ark AV, Shen H, Jones RG, et al. PGC-1β maintains mitochondrial metabolism and restrains inflammatory gene expression [Internet]. 2022. Available from: http://dx.doi.org/10.1101/2022.05.18.492477

40. Everts B, Amiel E, Huang SC-C, Smith AM, Chang C-H, Lam WY, et al. TLR-driven early glycolytic reprogramming via the kinases TBK1-IKKε supports the anabolic demands of dendritic cell activation. Nat Immunol. 2014 Apr;15(4):323–32.

41. Cunningham JT, Rodgers JT, Arlow DH, Vazquez F, Mootha VK, Puigserver P. mTOR controls mitochondrial oxidative function through a YY1–PGC-1α transcriptional complex. Nature. 2007 Nov 29;450(7170):736–40.

42. Edelson BT, Bradstreet TR, Hildner K, Carrero JA, Frederick KE, Kc W, et al. CD8α(+) dendritic cells are an obligate cellular entry point for productive infection by Listeria monocytogenes. Immunity. 2011 Aug 26;35(2):236–48.

43. Leylek R, Alcántara-Hernández M, Lanzar Z, Lüdtke A, Perez OA, Reizis B, et al. Integrated Cross-Species Analysis Identifies a Conserved Transitional Dendritic Cell Population. Cell Rep. 2019 Dec 10;29(11):3736-3750.e8.

44. Merad M, Sathe P, Helft J, Miller J, Mortha A. The dendritic cell lineage: ontogeny and function of dendritic cells and their subsets in the steady state and the inflamed setting. Annu Rev Immunol. 2013;31:563–604.

45. Ginhoux F, Guilliams M, Merad M. Expanding dendritic cell nomenclature in the single-cell era. Nat

Rev Immunol. 2022 Feb;22(2):67–8.

46. Pelayo R, Hirose J, Huang J, Garrett KP, Delogu A, Busslinger M, et al. Derivation of 2 categories of plasmacytoid dendritic cells in murine bone marrow. Blood. 2005 Jun 1;105(11):4407–15.

47. Macal M, Jo Y, Dallari S, Chang AY, Dai J, Swaminathan S, et al. Self-Renewal and Toll-like Receptor Signaling Sustain Exhausted Plasmacytoid Dendritic Cells during Chronic Viral Infection. Immunity. 2018 Apr 17;48(4):730-744.e5.

48. Zuniga EI, Liou L-Y, Mack L, Mendoza M, Oldstone MBA. Persistent virus infection inhibits type I interferon production by plasmacytoid dendritic cells to facilitate opportunistic infections. Cell Host Microbe. 2008 Oct 16;4(4):374–86.

49. Liu H, Zhai L, Liu Y, Lu D, VanderArk A, Yang T, et al. The histone demethylase KDM5C controls female bone mass by promoting energy metabolism in osteoclasts. bioRxivorg [Internet]. 2023 Feb 23; Available from: http://dx.doi.org/10.1101/2023.02.23.529728

50. Liu X, Secombe J. The Histone Demethylase KDM5 Activates Gene Expression by Recognizing Chromatin Context through Its PHD Reader Motif. Cell Rep. 2015 Dec 15;13(10):2219–31.

51. Scandaglia M, Lopez-Atalaya JP, Medrano-Fernandez A, Lopez-Cascales MT, Del Blanco B, Lipinski M, et al. Loss of Kdm5c Causes Spurious Transcription and Prevents the Fine-Tuning of Activity-Regulated Enhancers in Neurons. Cell Rep. 2017 Oct 3;21(1):47–59.

52. Lança T, Ungerbäck J, Da Silva C, Joeris T, Ahmadi F, Vandamme J, et al. IRF8 deficiency induces the transcriptional, functional, and epigenetic reprogramming of cDC1 into the cDC2 lineage. Immunity. 2022 Aug 9;55(8):1431-1447.e11.

53. Villar J, Segura E. Decoding the Heterogeneity of Human Dendritic Cell Subsets. Trends Immunol. 2020 Dec;41(12):1062–71.

54. Brodin P, Davis MM. Human immune system variation. Nat Rev Immunol. 2017 Jan;17(1):21–9.

55. Granot T, Senda T, Carpenter DJ, Matsuoka N, Weiner J, Gordon CL, et al. Dendritic Cells Display Subset and Tissue-Specific Maturation Dynamics over Human Life. Immunity. 2017 Mar 21;46(3):504–15.

56. Papaioannou N. Environmental Signals Rather Than Layered Ontogeny Imprint the Function of Type 2 Conventional Dendritic Cells in Young and Adult Mice. München, Ludwig-Maximilians-Universität; 2021.

57. Iwase S, Brookes E, Agarwal S, Badeaux AI, Ito H, Vallianatos CN, et al. A Mouse Model of X-linked Intellectual Disability Associated with Impaired Removal of Histone Methylation. Cell Rep. 2016 Feb 9;14(5):1000–9.

58. Kirkling ME, Cytlak U, Lau CM, Lewis KL, Resteu A, Khodadadi-Jamayran A, et al. Notch Signaling Facilitates In Vitro Generation of Cross-Presenting Classical Dendritic Cells. Cell Rep. 2018 Jun 19;23(12):3658-3672.e6.

59. Corces MR, Trevino AE, Hamilton EG, Greenside PG, Sinnott-Armstrong NA, Vesuna S, et al. An improved ATAC-seq protocol reduces background and enables interrogation of frozen tissues. Nat Methods. 2017 Oct;14(10):959–62.

60. Buenrostro JD, Giresi PG, Zaba LC, Chang HY, Greenleaf WJ. Transposition of native chromatin for fast and sensitive epigenomic profiling of open chromatin, DNA-binding proteins and nucleosome position. Nat Methods. 2013 Dec;10(12):1213–8.

61. Li H. Aligning sequence reads, clone sequences and assembly contigs with BWA-MEM [Internet]. arXiv [q-bio.GN]. 2013. Available from: http://arxiv.org/abs/1303.3997

62. Faust GG, Hall IM. SAMBLASTER: fast duplicate marking and structural variant read extraction. Bioinformatics. 2014 Sep 1;30(17):2503–5.

63. Handsaker B, Wysoker A, Fennell T, Ruan J, Homer N. … Genome Project Data Processing Subgroup1000 Genome Project Data Processing Subgroup (2009) The sequence alignment/map format and SAMtools. Bioinformatics.

64. Ramírez F, Ryan DP, Grüning B, Bhardwaj V, Kilpert F, Richter AS, et al. deepTools2: a next generation web server for deep-sequencing data analysis. Nucleic Acids Res. 2016 Jul 8;44(W1):W160-5.

65. Amemiya HM, Kundaje A, Boyle AP. The ENCODE Blacklist: Identification of Problematic Regions of the Genome. Sci Rep. 2019 Jun 27;9(1):9354.

66. Stark R, Brown G, Others. DiffBind: differential binding analysis of ChIP-Seq peak data. R package version [Internet]. 2011;100(4.3). Available from: https://www.andersvercelli.com/packages/2.13/bioc/vignettes/DiffBind/inst/doc/DiffBind.pdf

67. Love MI, Huber W, Anders S. Moderated estimation of fold change and dispersion for RNA-seq data with DESeq2. Genome Biol. 2014;15(12):550.

68. Stephens M. False discovery rates: a new deal. Biostatistics. 2017 Apr 1;18(2):275–94.

69. Yu G, Wang L-G, Han Y, He Q-Y. clusterProfiler: an R package for comparing biological themes among gene clusters. OMICS. 2012 May;16(5):284–7.

70. Skene PJ, Henikoff S. An efficient targeted nuclease strategy for high-resolution mapping of DNA binding sites. Elife [Internet]. 2017 Jan 16;6. Available from: http://dx.doi.org/10.7554/eLife.21856

71. Zhang Z, Hernandez K, Savage J, Li S, Miller D, Agrawal S, et al. Uniform genomic data analysis in the NCI Genomic Data Commons. Nat Commun. 2021 Feb 22;12(1):1226.

72. Wilson SL, Shen SY, Harmon L, Burgener JM, Triche T Jr, Bratman SV, et al. Sensitive and reproducible cell-free methylome quantification with synthetic spike-in controls. Cell Rep Methods. 2022 Sep 19;2(9):100294.

73. Li H, Handsaker B, Wysoker A, Fennell T, Ruan J, Homer N, et al. The Sequence Alignment/Map format and SAMtools. Bioinformatics. 2009 Aug 15;25(16):2078–9.

74. Zhang Y, Liu T, Meyer CA, Eeckhoute J, Johnson DS, Bernstein BE, et al. Model-based analysis of ChIP-Seq (MACS). Genome Biol. 2008 Sep 17;9(9):R137.

75. Zerbino DR, Johnson N, Juettemann T, Wilder SP, Flicek P. WiggleTools: parallel processing of large collections of genome-wide datasets for visualization and statistical analysis. Bioinformatics. 2014 Apr 1;30(7):1008–9.

76. Ross-Innes CS, Stark R, Teschendorff AE, Holmes KA, Ali HR, Dunning MJ, et al. Differential oestrogen receptor binding is associated with clinical outcome in breast cancer. Nature. 2012 Jan 4;481(7381):389–93.

77. Yu G, Wang L-G, He Q-Y. ChIPseeker: an R/Bioconductor package for ChIP peak annotation, comparison and visualization. Bioinformatics. 2015 Jul 15;31(14):2382–3.

78. Heinz S, Benner C, Spann N, Bertolino E, Lin YC, Laslo P, et al. Simple combinations of lineage-determining transcription factors prime cis-regulatory elements required for macrophage and B cell identities. Mol Cell. 2010 May 28;38(4):576–89.

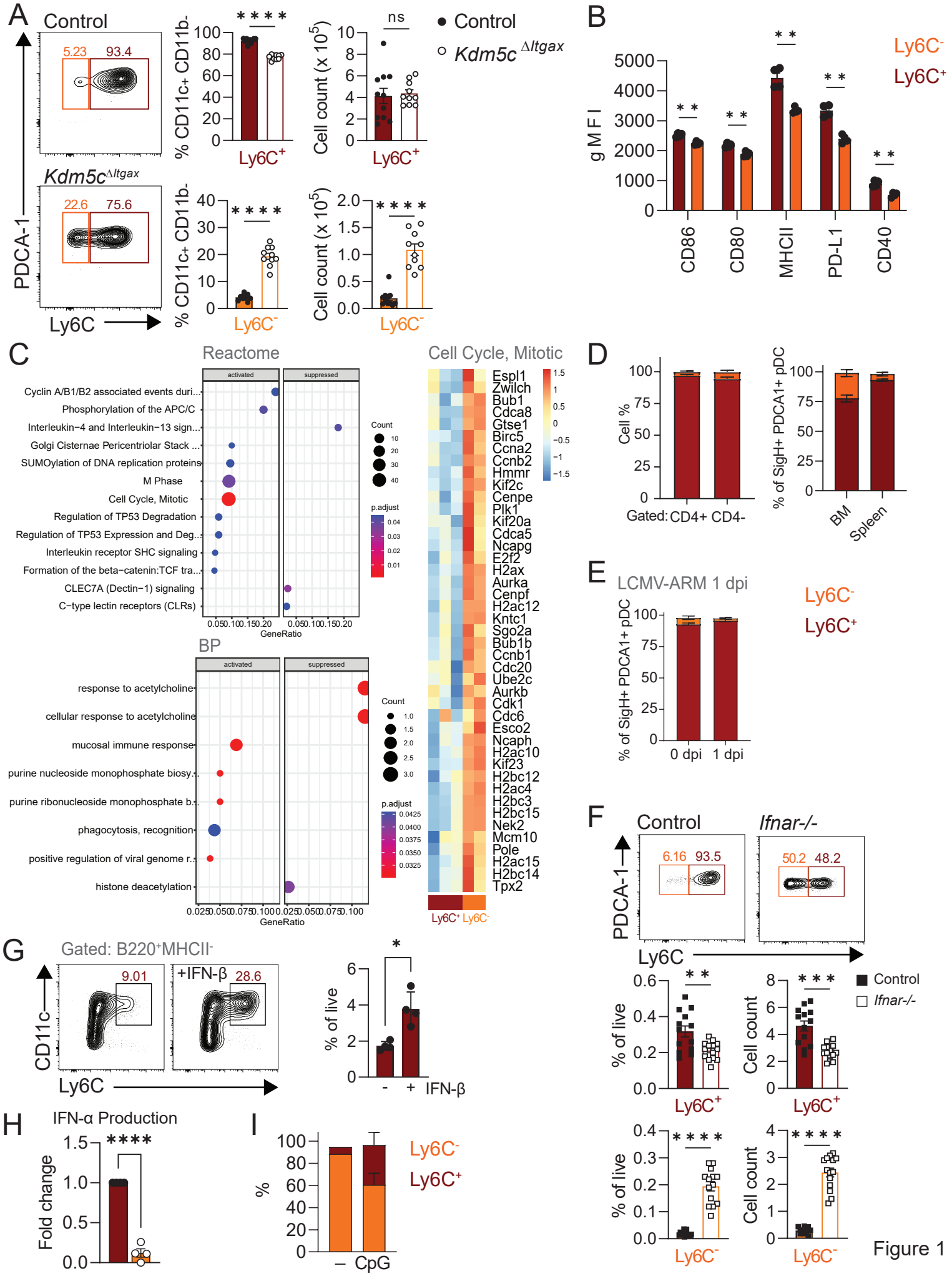
A
Control
5.23
93.4
Kdm5c ΔItgax
22.6
75.6
PDCA-1
Ly6C
% CD11c+ CD11b-
Cell count (x 10^5)
Ly6C+
Ly6C-
ns
Control
Kdm5c ΔItgax
B
gMFI
Ly6C-
Ly6C+
CD86
CD80
MHCII
PD-L1
CD40
C
Reactome
activated
suppressed
Cyclin A/B1/B2 associated events duri...
Phosphorylation of the APC/C
Interleukin−4 and Interleukin−13 sign...
Golgi Cisternae Pericentriolar Stack ...
SUMOylation of DNA replication proteins
M Phase
Cell Cycle, Mitotic
Regulation of TP53 Degradation
Regulation of TP53 Expression and Deg...
Interleukin receptor SHC signaling
Formation of the beta−catenin:TCF tra...
CLEC7A (Dectin−1) signaling
C−type lectin receptors (CLRs)
GeneRatio
Count
p.adjust
BP
response to acetylcholine
cellular response to acetylcholine
mucosal immune response
purine nucleoside monophosphate biosy...
purine ribonucleoside monophosphate b...
phagocytosis, recognition
positive regulation of viral genome r...
histone deacetylation
Cell Cycle, Mitotic
Espl1
Zwilch
Bub1
Cdca8
Gtse1
Birc5
Ccna2
Ccnb2
Hmmr
Kif2c
Cenpe
Plk1
Kif20a
Cdca5
Ncapg
E2f2
H2ax
Aurka
Cenpf
H2ac12
Kntc1
Sgo2a
Bub1b
Ccnb1
Cdc20
Ube2c
Aurkb
Cdk1
Cdc6
Esco2
Ncaph
H2ac10
Kif23
H2bc12
H2ac4
H2bc3
H2bc15
Nek2
Mcm10
Pole
H2ac15
H2bc14
Tpx2
Ly6C+ Ly6C-
D
Cell %
Gated: CD4+ CD4-
% of SigH+ PDCA1+ pDC
BM
Spleen
E
LCMV-ARM 1 dpi
% of SigH+ PDCA1+ pDC
0 dpi
1 dpi
Ly6C-
Ly6C+
F
Control
Ifnar-/-
6.16
93.5
50.2
48.2
PDCA-1
Ly6C
% of live
Cell count
Control
Ifnar-/-
Ly6C+
Ly6C-
G
Gated: B220+MHCII-
9.01
+IFN-β
28.6
CD11c
Ly6C
% of live
IFN-β
H
IFN-α Production
Fold change
I
%
CpG
Ly6C-
Ly6C+

Figure 1

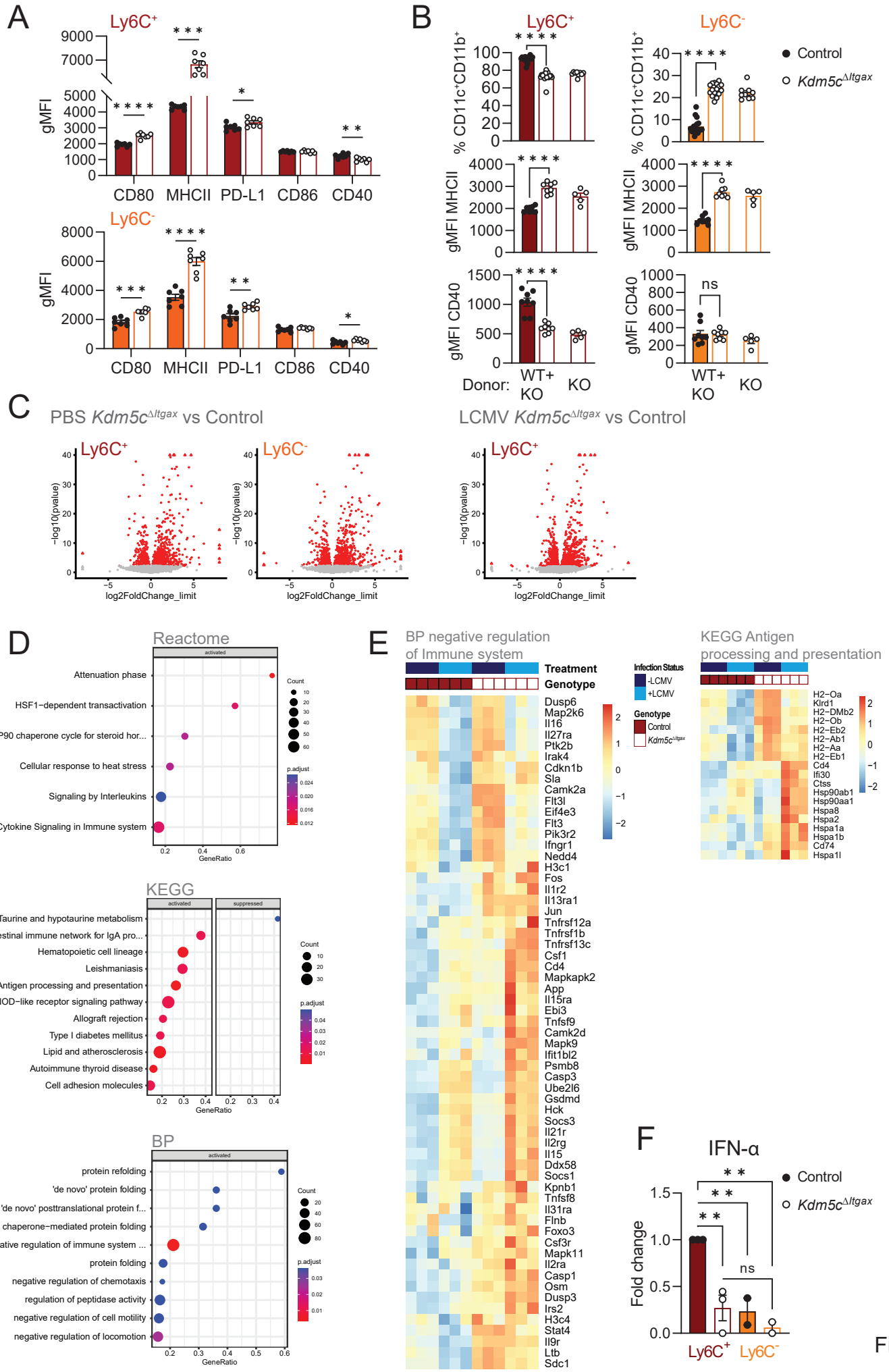
A
Ly6C+
gMFI
CD80
MHCII
PD-L1
CD86
CD40
Ly6C-
B
Ly6C+
Ly6C-
% CD11c+CD11b+
gMFI MHCII
gMFI CD40
Control
Kdm5cΔltgax
ns
Donor:
WT+ KO
KO
C
PBS Kdm5cΔltgax vs Control
LCMV Kdm5cΔltgax vs Control
−log10(pvalue)
log2FoldChange_limit
D
Reactome
activated
Attenuation phase
HSF1−dependent transactivation
HSP90 chaperone cycle for steroid hor...
Cellular response to heat stress
Signaling by Interleukins
Cytokine Signaling in Immune system
GeneRatio
Count
p.adjust
KEGG
suppressed
Taurine and hypotaurine metabolism
Intestinal immune network for IgA pro...
Hematopoietic cell lineage
Leishmaniasis
Antigen processing and presentation
NOD−like receptor signaling pathway
Allograft rejection
Type I diabetes mellitus
Lipid and atherosclerosis
Autoimmune thyroid disease
Cell adhesion molecules
BP
protein refolding
'de novo' protein folding
'de novo' posttranslational protein f...
chaperone−mediated protein folding
negative regulation of immune system ...
protein folding
negative regulation of chemotaxis
regulation of peptidase activity
negative regulation of cell motility
negative regulation of locomotion
E
BP negative regulation of Immune system
Treatment
Genotype
Infection Status
-LCMV
+LCMV
Control
Kdm5cΔltgax
Dusp6
Map2k6
Il16
Il27ra
Ptk2b
Irak4
Cdkn1b
Sla
Camk2a
Flt3l
Eif4e3
Flt3
Pik3r2
Ifngr1
Nedd4
H3c1
Fos
Il1r2
Il13ra1
Jun
Tnfrsf12a
Tnfrsf1b
Tnfrsf13c
Csf1
Cd4
Mapkapk2
App
Il15ra
Ebi3
Tnfsf9
Camk2d
Mapk9
Ifit1bl2
Psmb8
Casp3
Ube2l6
Gsdmd
Hck
Socs3
Il21r
Il2rg
Il15
Ddx58
Socs1
Kpnb1
Tnfsf8
Il31ra
Flnb
Foxo3
Csf3r
Mapk11
Il2ra
Casp1
Osm
Dusp3
Irs2
H3c4
Stat4
Il9r
Ltb
Sdc1
KEGG Antigen processing and presentation
H2−Oa
Klrd1
H2−DMb2
H2−Ob
H2−Eb2
H2−Ab1
H2−Aa
H2−Eb1
Cd4
Ifi30
Ctss
Hsp90ab1
Hsp90aa1
Hspa8
Hspa2
Hspa1a
Hspa1b
Cd74
Hspa1l
F
IFN-α
Fold change
Control
Kdm5cΔltgax
Ly6C+
Ly6C-

Figure 2

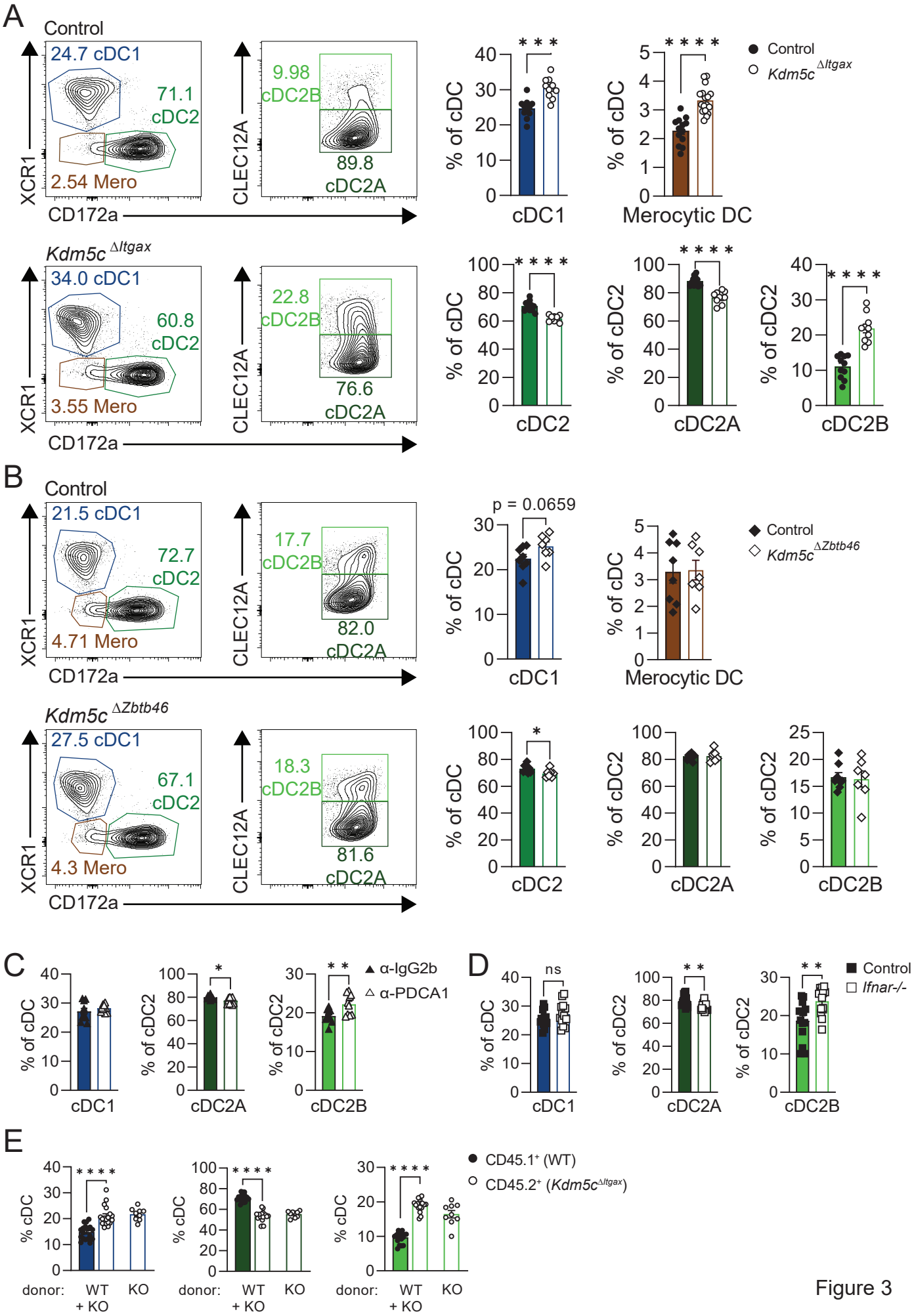
A
Control
24.7 cDC1
71.1 cDC2
2.54 Mero
XCR1
CD172a
9.98 cDC2B
89.8 cDC2A
CLEC12A
% of cDC
cDC1
Merocytic DC
Control
Kdm5c ΔItgax
Kdm5c ΔItgax
34.0 cDC1
60.8 cDC2
3.55 Mero
22.8 cDC2B
76.6 cDC2A
% of cDC2
cDC2
cDC2A
cDC2B
B
Control
21.5 cDC1
72.7 cDC2
4.71 Mero
17.7 cDC2B
82.0 cDC2A
p = 0.0659
Control
Kdm5c ΔZbtb46
Kdm5c ΔZbtb46
27.5 cDC1
67.1 cDC2
4.3 Mero
18.3 cDC2B
81.6 cDC2A
C
α-IgG2b
α-PDCA1
D
ns
Control
Ifnar-/-
E
CD45.1+ (WT)
CD45.2+ (Kdm5c ΔItgax)
donor: WT + KO
KO

Figure 3

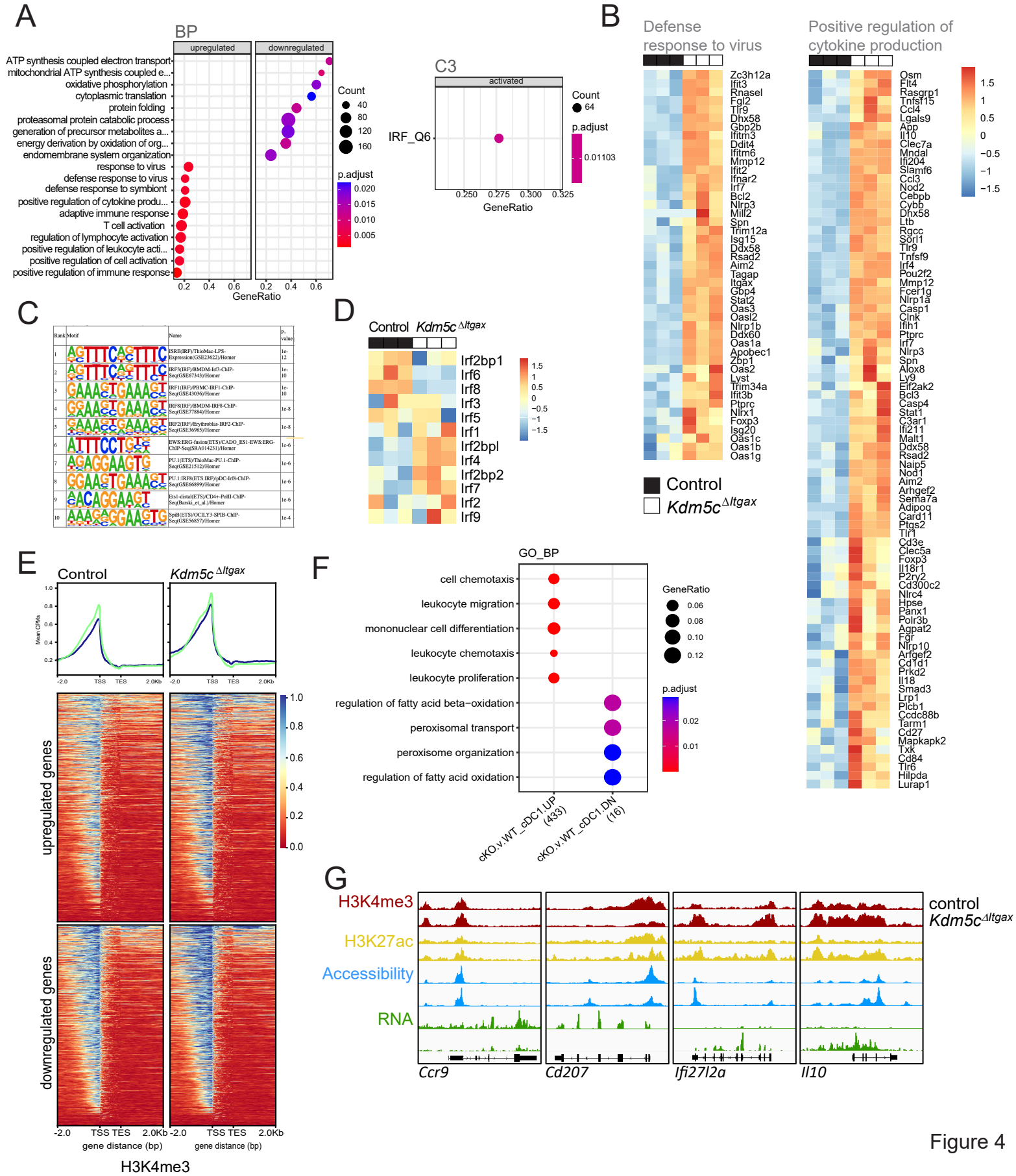
A
BP
upregulated
downregulated
ATP synthesis coupled electron transport
mitochondrial ATP synthesis coupled e...
oxidative phosphorylation
cytoplasmic translation
protein folding
proteasomal protein catabolic process
generation of precursor metabolites a...
energy derivation by oxidation of org...
endomembrane system organization
response to virus
defense response to virus
defense response to symbiont
positive regulation of cytokine produ...
adaptive immune response
T cell activation
regulation of lymphocyte activation
positive regulation of leukocyte acti...
positive regulation of cell activation
positive regulation of immune response
GeneRatio
Count
40
80
120
160
p.adjust
0.020
0.015
0.010
0.005
C3
activated
IRF_Q6
0.250
0.275
0.300
0.325
GeneRatio
Count
64
p.adjust
0.01103
B
Defense response to virus
Positive regulation of cytokine production
Control
Kdm5c Δltgax
C
Rank
Motif
Name
P-value
D
Control
Kdm5c Δltgax
Irf2bp1
Irf6
Irf8
Irf3
Irf5
Irf1
Irf2bpl
Irf4
Irf2bp2
Irf7
Irf2
Irf9
E
Control
Kdm5c Δltgax
Mean CPM/s
TSS
TES
2.0Kb
upregulated genes
downregulated genes
gene distance (bp)
H3K4me3
F
GO_BP
cell chemotaxis
leukocyte migration
mononuclear cell differentiation
leukocyte chemotaxis
leukocyte proliferation
regulation of fatty acid beta−oxidation
peroxisomal transport
peroxisome organization
regulation of fatty acid oxidation
cKO.v.WT_cDC1.UP (433)
cKO.v.WT_cDC1.DN (16)
GeneRatio
0.06
0.08
0.10
0.12
p.adjust
0.02
0.01
G
H3K4me3
H3K27ac
Accessibility
RNA
control
Kdm5c Δltgax
Ccr9
Cd207
Ifi27l2a
Il10

Figure 4

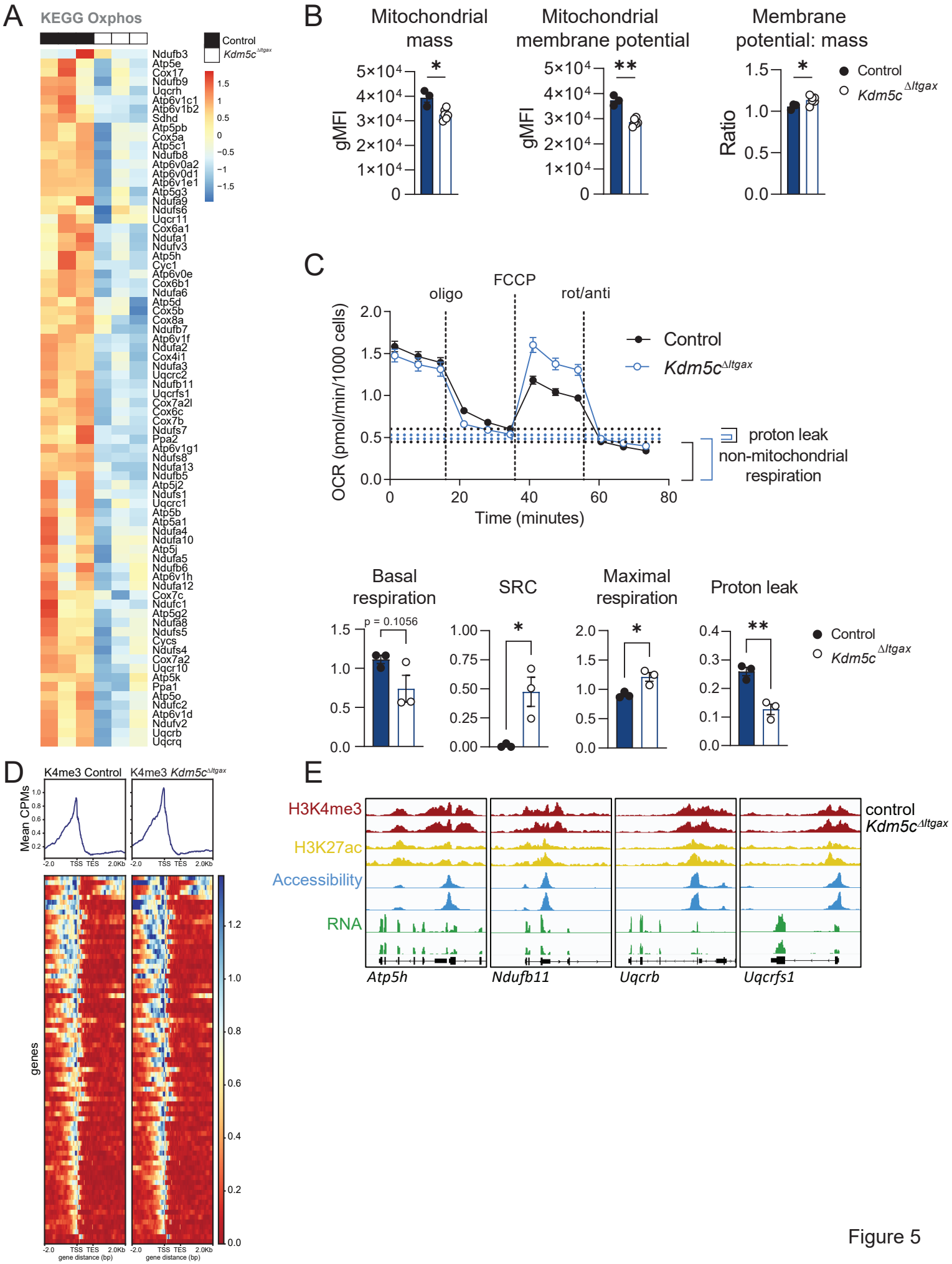
A
KEGG Oxphos
Control
Kdm5c Δltgax
Ndufb3
Atp5e
Cox17
Ndufb9
Uqcrh
Atp6v1c1
Atp6v1b2
Sdhd
Atp5pb
Cox5a
Atp5c1
Ndufb8
Atp6v0a2
Atp6v0d1
Atp6v1e1
Atp5g3
Ndufa9
Ndufs6
Uqcr11
Cox6a1
Ndufa1
Ndufv3
Atp5h
Cyc1
Atp6v0e
Cox6b1
Ndufa6
Atp5d
Cox5b
Cox8a
Ndufb7
Atp6v1f
Ndufa2
Cox4i1
Ndufa3
Uqcrc2
Ndufb11
Uqcrfs1
Cox7a2l
Cox6c
Cox7b
Ndufs7
Ppa2
Atp6v1g1
Ndufs8
Ndufa13
Ndufb5
Atp5j2
Ndufs1
Uqcrc1
Atp5b
Atp5a1
Ndufa4
Ndufa10
Atp5j
Ndufa5
Ndufb6
Atp6v1h
Ndufa12
Cox7c
Ndufc1
Atp5g2
Ndufa8
Ndufs5
Cycs
Ndufs4
Cox7a2
Uqcr10
Atp5k
Ppa1
Atp5o
Ndufc2
Atp6v1d
Ndufv2
Uqcrb
Uqcrq
B
Mitochondrial mass
Mitochondrial membrane potential
Membrane potential: mass
gMFI
Ratio
Control
Kdm5c Δltgax
C
FCCP
oligo
rot/anti
OCR (pmol/min/1000 cells)
Time (minutes)
proton leak
non-mitochondrial respiration
Basal respiration
SRC
Maximal respiration
Proton leak
p = 0.1056
D
K4me3 Control
K4me3 Kdm5c Δltgax
Mean CPMs
genes
gene distance (bp)
E
H3K4me3
H3K27ac
Accessibility
RNA
control
Kdm5c Δltgax
Atp5h
Ndufb11
Uqcrb
Uqcrfs1

Figure 5

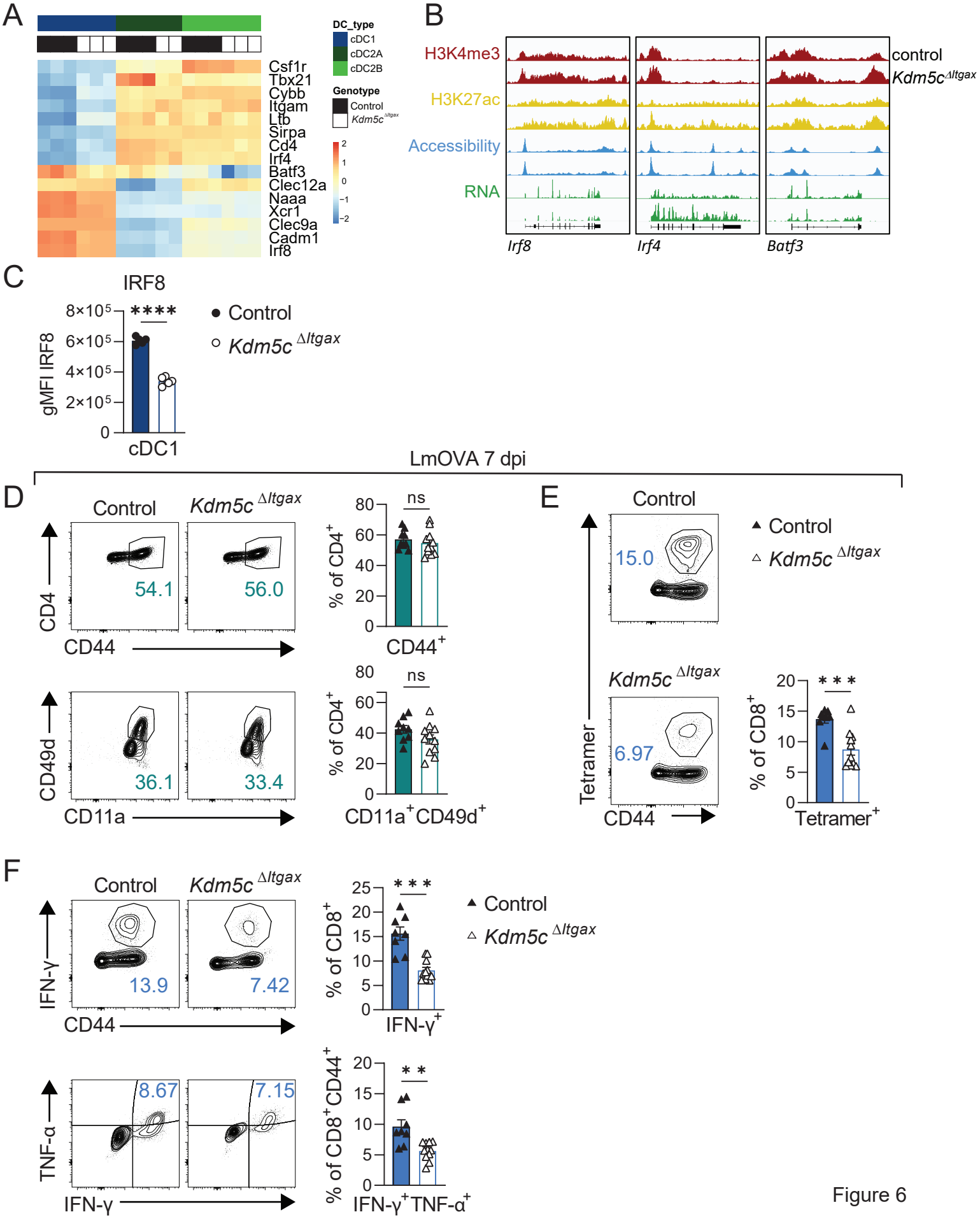
A
DC_type
cDC1
cDC2A
cDC2B
Genotype
Control
Kdm5c ΔItgax
Csf1r
Tbx21
Cybb
Itgam
Ltb
Sirpa
Cd4
Irf4
Batf3
Clec12a
Naaa
Xcr1
Clec9a
Cadm1
Irf8
B
H3K4me3
H3K27ac
Accessibility
RNA
control
Kdm5c ΔItgax
Irf8
Irf4
Batf3
C
IRF8
gMFI IRF8
8×10^5
6×10^5
4×10^5
2×10^5
0
****
cDC1
Control
Kdm5c ΔItgax
LmOVA 7 dpi
D
Control
Kdm5c ΔItgax
CD4
CD44
54.1
56.0
% of CD4+
ns
CD44+
CD49d
CD11a
36.1
33.4
CD11a+CD49d+
E
Control
15.0
Kdm5c ΔItgax
6.97
Tetramer
CD44
% of CD8+
***
Tetramer+
F
Control
Kdm5c ΔItgax
IFN-γ
CD44
13.9
7.42
% of CD8+
IFN-γ+
TNF-α
IFN-γ
8.67
7.15
% of CD8+CD44+
**
IFN-γ+TNF-α+

Figure 6